Am J Physiol Cell Physiol 300: C1047–C1054, 2011.
First published January 26, 2011; doi:10.1152/ajpcell.00416.2010.

4F2hc stabilizes GLUT1 protein and increases glucose transport activity

Haruya Ohno,[1] Yusuke Nakatsu,[1] Hideyuki Sakoda,[2] Akifumi Kushiyama,[3] Hiraku Ono,[2] Midori Fujishiro,[2] Yuichiro Otani,[1] Hirofumi Okubo,[1] Masayasu Yoneda,[1] Toshiaki Fukushima,[1] Yoshihiro Tsuchiya,[1] Hideaki Kamata,[1] Fusanori Nishimura,[4] Hiroki Kurihara,[5] Hideki Katagiri,[6] Yoshitomo Oka,[6] and Tomoichiro Asano[1]

[1]*Department of Medical Science, Graduate School of Medicine, University of Hiroshima, Hiroshima, Japan;* [2]*Department of Internal Medicine, Graduate School of Medicine, University of Tokyo, Tokyo, Japan;* [3]*Institute for Adult Disease, Asahi Life Foundation, Tokyo, Japan;* [4]*Department of Dental Science for Health Promotion, Hiroshima University Graduate School of Biomedical Sciences, Hiroshima, Japan;* [5]*Department of Physiological Chemistry and Metabolism, Graduate School of Medicine, University of Tokyo, Tokyo, Japan; and* [6]*Division of Molecular Metabolism and Diabetes, Tohoku University Graduate School of Medicine, Sendai, Japan*

Submitted 12 October 2010; accepted in final form 13 January 2011

Ohno H, Nakatsu Y, Sakoda H, Kushiyama A, Ono H, Fujishiro M, Otani Y, Okubo H, Yoneda M, Fukushima T, Tsuchiya Y, Kamata H, Nishimura F, Kurihara H, Katagiri H, Oka Y, Asano T. 4F2hc stabilizes GLUT1 protein and increases glucose transport activity. *Am J Physiol Cell Physiol* 300: C1047–C1054, 2011. First published January 26, 2011; doi:10.1152/ajpcell.00416.2010.—Glucose transporter 1 (GLUT1) is widely distributed throughout various tissues and contributes to insulin-independent basal glucose uptake. Using a split-ubiquitin membrane yeast two-hybrid system, we newly identified 4F2 heavy chain (4F2hc) as a membrane protein interacting with GLUT1. Though 4F2hc reportedly forms heterodimeric complexes between amino acid transporters, such as LAT1 and LAT2, and regulates amino acid uptake, we investigated the effects of 4F2hc on GLUT1 expression and the associated glucose uptake. First, FLAG-tagged 4F2hc and hemagglutinin-tagged GLUT1 were overexpressed in human embryonic kidney 293 cells and their association was confirmed by coimmunoprecipitation. The green fluorescent protein-tagged 4F2hc and DsRed-tagged GLUT1 showed significant, but incomplete, colocalization at the plasma membrane. In addition, an endogenous association between GLUT1 and 4F2hc was demonstrated using mouse brain tissue and HeLa cells. Interestingly, overexpression of 4F2hc increased the amount of GLUT1 protein in HeLa and HepG2 cells with increased glucose uptake. In contrast, small interfering RNA (siRNA)-mediated 4F2hc gene suppression markedly reduced GLUT1 protein in both cell types, with reduced glucose uptake. While GLUT1 mRNA levels were not affected by overexpression or gene silencing of 4F2hc, GLUT1 degradation after the addition of cycloheximide was significantly suppressed by 4F2hc overexpression and increased by 4F2hc siRNA treatment. Taken together, these observations indicate that 4F2hc is likely to be involved in GLUT1 stabilization and to contribute to the regulation of not only amino acid but also glucose metabolism.

4F2 heavy chain; glucose transporter 1; glucose uptake

GLUCOSE IS A MAJOR SOURCE of energy for nearly all living organisms, and the system for its efficient transport into cells is highly conserved from simple bacteria to mammalian cells. The facilitative glucose transporters (GLUTs) constitute an energy-independent system that transports D-glucose down a concentration gradient. GLUT1, the first GLUT identified, was purified from the red blood cell membrane and has a structure consisting of 12 transmembrane domains that delineate six extracellular loops (26). Since the discovery of GLUT1, another 13 GLUT isoforms, which are involved in glucose or fructose transport, have been identified in mammals. Among the isoforms identified to date, GLUT1 is widely distributed throughout nearly all tissues and is generally present in the plasma membrane regardless of whether stimulation is delivered. In addition, since it possesses a high affinity for D-glucose, GLUT1 is regarded as contributing mainly to basal glucose uptake.

Elevated GLUT1 expression has been shown in many cancers (3, 37). Oncogenes such as Ras and Src have been shown to upregulate GLUT1 expression (4, 9). In addition, hypoxia-inducible factor 1 , c-Myc, Akt, and estrogen have been shown to induce GLUT1 expression (11, 36). In contrast, the mechanism regulating the intrinsic activity or stability of GLUT remains largely unknown.

In this study, on the basis of the hypothesis that certain protein(s) bind to and alter the function of GLUT1, we attempted to identify a protein binding with GLUT proteins. Since the conventional yeast two-hybrid system is not suitable for detecting interactions between membrane proteins, we employed the newly developed split-ubiquitin membrane yeast two-hybrid system, which allows the interactions between an integral membrane protein and its partner(s) to be detected (38). Interestingly, screening using GLUT1 as bait yielded the cDNA encoding the heavy chain (hc) of 4F2, 4F2hc (CD98). 4F2hc reportedly forms a complex with LAT1 or LAT2, and this heterodimer (LAT1/4F2hc) functions as an amino acid transporter at the plasma membrane (14, 31, 33, 35). Herein, we show that 4F2hc also associates with GLUT1 and contributes to GLUT1 stability, leading to increased glucose transport activity into cells.

MATERIALS AND METHODS

Anti-4F2hc antibody was generated by immunization of rabbits with the glutathione *S*-transferase-fused COOH-terminal 103 amino acids of human 4F2hc. Anti-FLAG tag and anti-hemagglutinin (HA) tag antibodies were purchased from Sigma-Aldrich (St. Louis, MO). Anti-GLUT1 antibody was from Fabgennix (Mississauga, ON, Canada). Anti-LAT1, anti-4F2hc (mouse), anti-insulin Rβ, and anti-LexA antibodies were from Santa Cruz Biotechnology (Santa Cruz, CA). Anti-rabbit and anti-mouse horseradish peroxidase-conjugated antibodies were obtained from GE Healthcare (Buckinghamshire, UK). Dulbecco's modified Eagle's medium (DMEM) and fetal bovine

Address for reprint requests and other correspondence: T. Asano, Dept. of Medical Science, Graduate School of Medicine, Univ. of Hiroshima, 1-2-3 Kasumi, Minami-ku, Hiroshima City, Hiroshima, Japan 734-8553 (e-mail: asano-tky@umin.ac.jp).

serum were purchased from Invitrogen (Carlsbad, CA). 3FLAG-4F2hc cDNA was provided by Yoshikatsu Kanai. All other reagents were of analytical grade.

Split-ubiquitin membrane yeast two-hybrid screening system. DUALmembrane kit 3 (Dualsystems Biotech), the split-ubiquitin membrane yeast two-hybrid system, was used to identify the protein associating with GLUT1. Briefly, in this system, the bait is fused to the COOH-terminal half of ubiquitin (Cub) and the artificial transcription factor LexA-VP16. The prey is fused to the mutated NH_2-terminal half of ubiquitin (NubG). If the bait and prey interact, split ubiquitins are reconstituted and recognized by ubiquitin-specific proteases. Then, the artificial transcription factor consisting of Cub and LexA-VP16 is released and moves to the nucleus, leading to reporter gene activation (Fig. 1*A*).

Rabbit GLUT1 cDNA was inserted into the expression vector pBT3-STE to generate the fusion bait with the split ubiquitin and an artificial transcriptional factor (Cub-LexA-VP16) to the COOH terminus of GLUT1. Mouse heart cDNA library, inserted into a pDL2xN-SUC/pDL2xN-STE vector, was purchased from Dualsystems Biotech, and then screened. Bait and the mouse heart cDNA library were transformed into yeast strain NMY51. The HIS3 reporter construct was assayed by growth on SD-Trp-Leu-His-Ade drop-out plates supplemented with 2.5 mM 3-amino-1,2,4-triazole (Wako). Qualitative assessment of the lacZ reporter was conducted using filter lift galactosidase assays (8).

Cell culture, expression vectors, adenovirus generation, and small interfering RNA transfections. HepG2 hepatoma cells, HeLa cells, and human embryonic kidney (HEK293) cells were grown in DMEM containing 10% fetal calf serum at 37°C in 5% (vol/vol) CO_2 in air. Rabbit GLUT1-HA, rat GLUT4-HA, rabbit GLUT1-DsRed, human LAT1-DsRed, green fluorescent protein (GFP)-human 4F2hc, and human 4F2hc were inserted into cloning sites in the mammalian expression vector pcDNA3 (Invitrogen), as reported previously (34). Transfection of these expression vectors was performed by the lipofection method using FuGENE 6 (Roche Applied Science, Indianapolis, IN). Recombinant adenovirus, encoding mouse 4F2hc, was generated according to the instruction manual of the Adenovirus Dual Expression Kit (TaKaRa Bio). Adenovirus encoding LacZ served as a control.

The small interfering RNA (siRNA) against 4F2hc was purchased from Invitrogen (Stealth/siRNA duplex oligoribonucleotides), and the transfection of this siRNA was performed using Lipofectamine RNAiMAX (Invitrogen).

Immunoprecipitation and immunoblotting. Whole cell extracts were prepared from HEK293 cells overexpressing 3FLAG-4F2hc, GLUT1-HA, or GLUT4-HA in lysis buffer [50 mM Tris·HCl, pH 7.5, 150 mM NaCl, 10% (wt/vol) glycerol, 100 mM NaF, 10 mM EGTA, 1 mM Na_3VO_4, 1% (wt/vol) Triton X-100, 5 μM $ZnCl_2$, 2 mM phenylmethylsulfonyl fluoride (PMSF), 10 μg/ml aprotinin, and 1 μg/ml leupeptin]. Cell extracts were incubated for 4 h at 4°C with the HA antibody and then for 1 h with 30 μl of protein G-Sepharose beads. The pellets were washed five times with 1 ml of lysis buffer, resuspended in Laemmli sample buffer, and subjected to SDS-polyacrylamide gel electrophoresis (SDS-PAGE).

HeLa cells were preincubated with 2.5 mM DSP (Thermo Scientific) for 30 min. Male mice, 9 wk of age, were obtained from the Nippon Bio-Supply Center (Tokyo, Japan). All animal studies were conducted according to the Japanese guidelines for the care and use of experimental animals, and the experimental protocols were approved by the Committee of Research Facilities for Laboratory Animal Science, Natural Science Center for Basic Research and Development (N-BARD), University of Hiroshima. For preparation of the membrane fraction, HeLa cells and mouse whole brains were homogenized with homogenizing buffer (0.25 M sucrose, 10 mM Tris, 1 mM EDTA). After filtration through a nylon membrane, the lysates were centrifuged at 600 *g* for 10 min, and the supernatant was centrifuged at 3,000 *g* for 10 min. Then, the supernatant was centrifuged at 30,000 *g* for 30 min, and the pellet was resuspended in 10 mM Tris, 1 mM EDTA, at pH 7.4.

The 4F2hc antibody (90 μg) or control IgG (90 μg) was covalently coupled to 20 μl of IPeX beads (Gene Bio-Application) and stabilized for 30 min at room temperature. Then, the solubilized membrane fraction (200 μg in 200 μl) was incubated with 5 μl of anti-4F2hc-coupled or anti-IgG-coupled beads for 4 h at 4°C. The beads were extensively washed, and the immunoprecipitated proteins were eluted in Laemmli buffer and resolved by SDS-PAGE.

Western blot analysis was carried out as described previously (34). In brief, equal amounts of protein lysates were separated by SDS-PAGE and electrophoretically transferred to polyvinylidene difluoride membranes in a transfer buffer consisting of 20 mM Tris·HCl, 150 mM glycine, and 20% methanol. The membranes were blocked with 3% nonfat dry milk in Tris-buffered saline with 0.1% Tween 20 and incubated with specific antibodies, followed by incubation with horseradish peroxidase-conjugated secondary antibodies. The antigen-antibody interactions were visualized by incubation with ECL chemiluminescence reagent (GE Healthcare).

Measurement of 2-deoxyglucose and leucine uptakes. The 2-deoxy-D-[^{3}H]glucose uptake assay was performed as described previously (2). HeLa or HepG2 cells were incubated in serum-free DMEM for 2 h, rapidly washed at 37°C with KRP buffer (in mM: 128 NaCl, 4.7 KCl, 1.25 $CaCl_2$, 1.25 $MgSO_4$, 10 $NaHPO_4$, pH 7.4), and 450 μl of KRP buffer were then added to each well. The measurements of 2-deoxyglucose uptake were initiated by addition of 50 μl of 2-deoxy-D-[1, 2-^{3}H]glucose, so that each well contained 0.4 μCi and 0.1 mM 2-deoxyglucose. After a 5-min incubation at 37°C, 1 ml of ice-cold phosphate-buffered saline (PBS) containing 10 mM glucose and 0.3 mM phloretin was added, and the cells were rapidly washed three times with ice-cold PBS containing 10 mM glucose and subsequently solubilized by adding SDS (final concentration, 0.05%). Aliquots of the solubilized extract were assayed for radioactivity using a liquid scintillation counter.

The [^{14}C]L-leucine uptake experiments were performed by essentially the same method as those of 2-deoxy-D-[^{3}H]glucose uptake, with a few modifications (18). Instead of KRP buffer, Na^+-free uptake solution (in mM: 125 choline Cl, 4.8 KCl, 1.3 $CaCl_2$, 1.2 $MgSO_4$, 25 HEPES-Tris, 1.2 KH_2PO_4, 5.6 glucose, pH 7.4) was used. After a 1-min incubation with 20 μM (final concentration) [^{14}C]L-leucine, the uptake reaction was terminated by removing the uptake solution followed by washing four times with ice-cold uptake solution.

GLUT1 degradation assay. To observe GLUT1 degradation, 10 μg/μl cycloheximide, an inhibitor of protein synthesis, was added as indicated in RESULTS and figure legends. The GLUT1 expression level was measured by immunoblotting at the indicated time after the addition of cycloheximide. A lysosome inhibitor, chloroquine, 20 μM (Wako), and a proteasome inhibitor, MG-132, 10 μM (Sigma Aldrich), were added to HeLa cells, and their effects on GLUT1 degradation were also examined.

Immunostaining. HeLa cells were fixed with 4% paraformaldehyde for 10 min, rinsed with PBS, and then exposed to 0.2% Triton X-100 in PBS for 5 min. The cells were subsequently incubated for 1 h at room temperature with anti-GLUT1 rabbit antibody (1:100) and anti-4F2hc mouse antibody (1:50). After being washed with PBS five times, FITC-labeled anti-rabbit IgG (1:100) and Cy3-labeled anti-mouse IgG (1:100) were added as the secondary antibodies. Immunofluorescence was visualized with a laser-scanning confocal imaging system.

RNA analysis. RNA extractions were carried out using TRIzol followed by purification over a QIAEASY RNA column. Reverse transcription and quantitative PCR were carried out as already described. Amplifications of GLUT1 and GAPDH cDNAs were performed using the Opticon Monitor (version 3; Bio-Rad). Cycling conditions comprised a 3-min denaturation step at 95°C, followed by 40 cycles of denaturation (95°C for 15 s), annealing (60°C for 30 s),

and extension (72°C for 30 s). After amplification, melting curve analysis was performed. Each sample was amplified in triplicate.

The primer sets for human (h)GLUT1 were TCACTGTGCTCCTGGTTCTG and CCTGTGCTCCTGAGAGATCC (233 bp) and for hGAPDH were ACCACAGTCCATGCCATCAC and TCCACCACCCTGTTGCTGTA (451 bp).

Statistical analysis. Results are expressed as means ± SE, and statistical comparisons among groups were carried out using Student's *t*-test, unless otherwise indicated.

RESULTS

Identification of 4F2hc, as a novel membrane protein interacting with GLUT1, by the split-ubiquitin membrane yeast two-hybrid system. As bait, full-length GLUT1 was fused to the COOH-terminal half of ubiquitin (Cub) and artificial transcription factors. Expression of the bait in yeast was confirmed by immunoblotting against LexA (Fig. 1*B*). A mouse heart muscle cDNA library, fused to the mutated NH_2-terminal half of ubiquitin (NubG), was screened with the above-mentioned GLUT1 cDNA construct. After the exclusion of nonspecific positive clones, we newly identified 4F2hc as a membrane protein interacting with GLUT1. 4F2hc and GLUT1 coexpressing yeast proliferated in the selective plate (Fig. 1*C*) and exhibited robust β-galactosidase activity (Fig. 1*D*), indicating an interaction between 4F2hc and GLUT1 in yeast.

4F2hc associates and colocalizes with GLUT1. First, FLAG-tagged 4F2hc and either HA-tagged GLUT1 or HA-tagged GLUT4 were overexpressed in HEK293 cells and their associations were examined by coimmunoprecipitation (Fig. 2*A*).

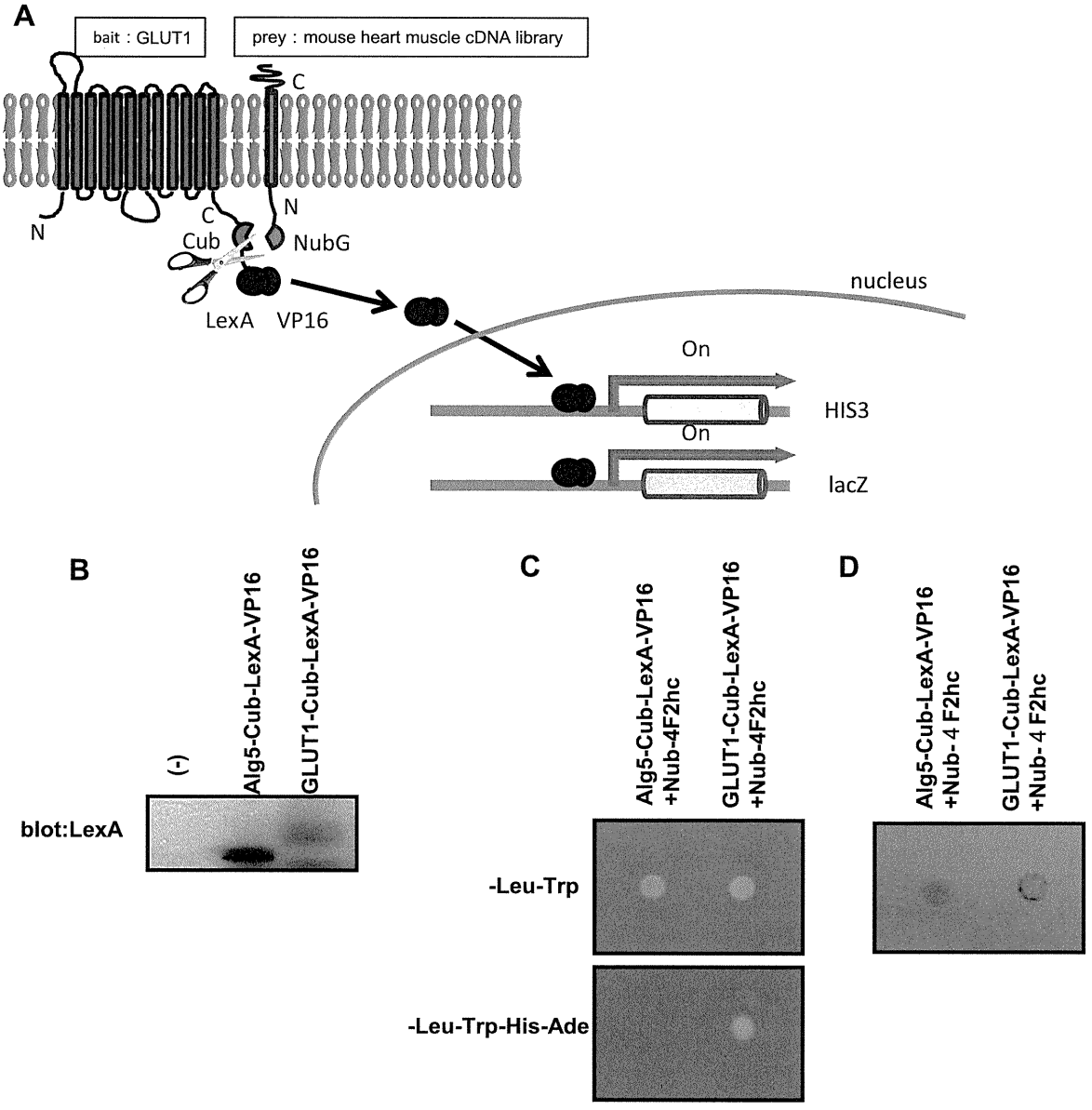

Fig. 1. Using the split-ubiquitin yeast two-hybrid system, 4F2hc was newly identified as a membrane protein interacting with glucose transporter 1 (GLUT1). *A*: split-ubiquitin yeast-two hybrid system. Full-length GLUT1 is fused to the COOH-terminal half of ubiquitin (Cub) and the artificial transcription factor LexA-VP16. Mouse heart muscle cDNA library is fused to the mutated NH_2-terminal half of ubiquitin (NubG). *B*: expression of GLUT1 as bait in yeast. Yeast was subjected to protein extraction before separation of proteins by SDS-PAGE. *C*: yeast coexpressed with Nub-4F2hc and either Alg5-Cub-LexA-VP16 or GLUT1-Cub-LexA-VP16 was incubated on a selective plate for 72 h. *D*: color development in a β-galactosidase assay.

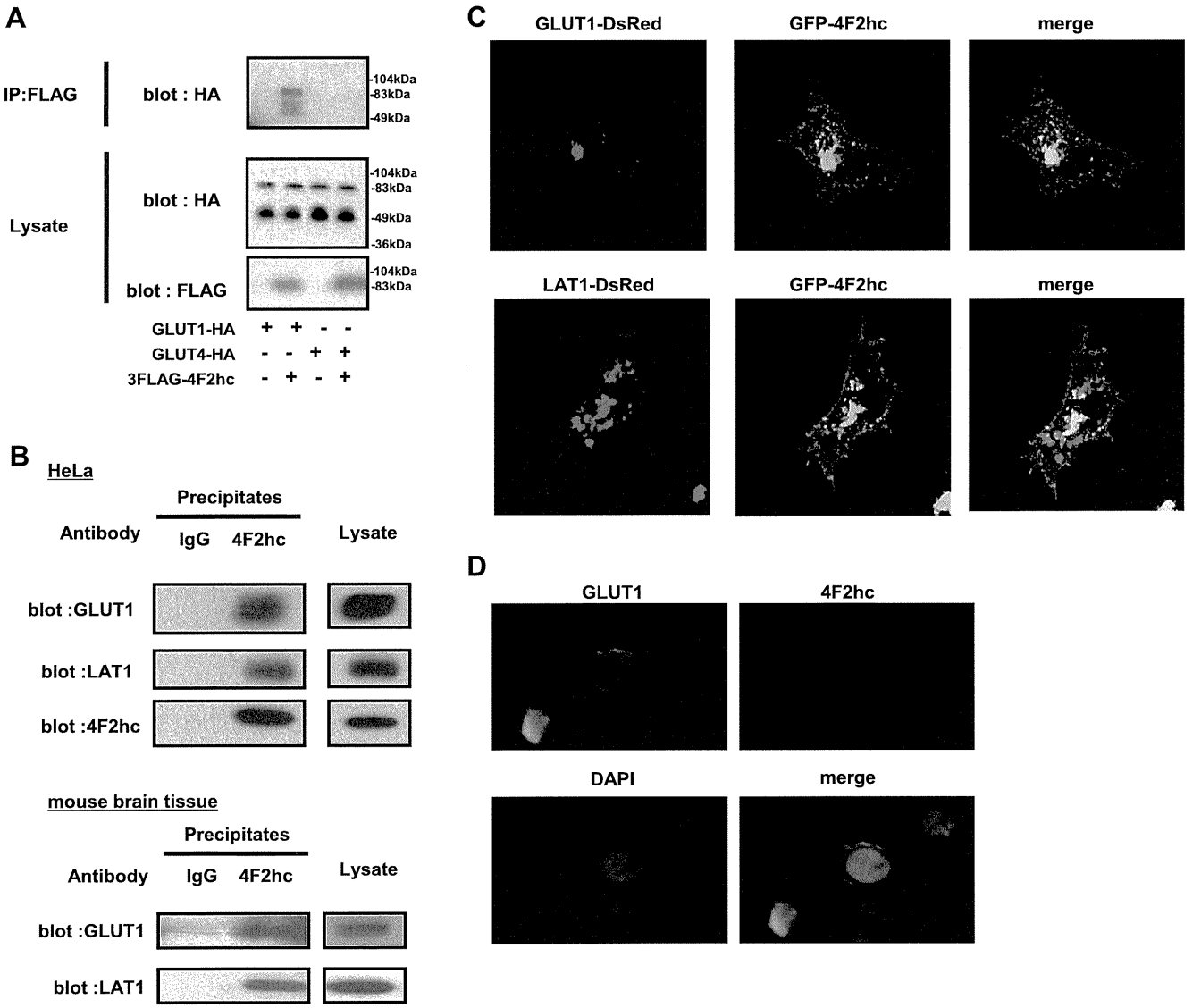

Fig. 2. 4F2hc associates with GLUT1 and shows colocalization with GLUT1. *A*: human embryonic kidney 293 (HEK293) cells were cotransfected with 3FLAG-4F2hc, GLUT1-hemagglutinin (HA), and GLUT4-HA expression plasmids. After 48 h, lysates were subjected to immunoprecipitation (IP) and immunoblotting. *B*: 4F2hc antibody was immobilized onto agarose beads (IPeX kit; Gene Bio-Application). The membrane fraction of HeLa cells (*top*) or mouse brain tissue (*bottom*) was added to the beads and immunoprecipitated. *C*: fluorescence images of HeLa cells cotransfected with green fluorescent protein (GFP)-4F2hc and either GLUT1-DsRed or LAT1-DsRed. *D*: immunostaining images, obtained using GLUT1 and CD98-specific antibodies in HeLa cells.

HA-tagged GLUT1 but not GLUT4 was detected in the FLAG-tagged 4F2hc immunoprecipitate. Next, we examined the association between endogenous GLUT1 and 4F2hc in HeLa cells and mouse brain, employing coimmunoprecipitation (Fig. 2*B*). GLUT1 was detected by the anti-4F2hc antibody, but not control IgG, in membrane fraction immunoprecipitates. The positive control, LAT1 in the anti-4F2hc antibody immunoprecipitate, was also confirmed in both HeLa cells and mouse brain.

Then, GFP-tagged 4F2hc and DsRed-tagged GLUT1 were transfected into HeLa cells, and colocalization of GLUT1 or LAT1 with 4F2hc was investigated. Considerable amounts of these GFP-tagged proteins appeared to be aggregated near nuclei and within intracellular vesicles, but LAT1 as well as GLUT1 apparently exhibited significant colocalization with 4F2hc at the plasma membrane and intracellular sites (Fig. 2*C*). In addition, endogenous GLUT1 and 4F2hc in HeLa cells were coimmunostained with anti-GLUT1 and anti-4F2hc antibodies (Fig. 2*D*). Although these staining data do not convincingly demonstrate an association between GLUT1 and 4F2hc, their colocalization at the plasma membrane raises this possibility.

Overexpression of 4F2hc increases glucose uptake. Since 4F2hc is likely to interact with GLUT1, the effect of 4F2hc on glucose transport activity was examined. 4F2hc reportedly regulates the functions of amino acid transporters, and increased 4F2hc expression enhances amino acid uptake. First, 4F2hc was overexpressed in HeLa cells, and the uptakes of 2-deoxyglucose and leucine were measured. Overexpression of

4F2hc increased glucose uptake in an expression level-dependent manner, by up to 55%, and leucine uptake was similarly increased (Fig. 3*B*). Interestingly, 4F2hc overexpression also increased the amount of GLUT1 protein (Fig. 3*A*). Since the transfection efficiency of the 4F2hc encoding plasmid in HepG2 cells was not sufficient, we employed adenovirus-mediated 4F2hc overexpression for HepG2 cells. Overexpression of 4F2hc by adenovirus in HepG2 cells also increased glucose uptake and the amount of GLUT1 protein (Fig. 3, *C* and *D*).

Knockdown of 4F2hc decreases glucose uptake and GLUT1 expression level. To further investigate the role of 4F2hc in glucose uptake, we performed loss of function analyses. Treatment with 4F2hc siRNA but not control siRNA reduced the 4F2hc protein expression level by ~90% (Fig. 4, *A* and *C*, *left*). Importantly, 4F2hc siRNA treatment also markedly reduced GLUT1 protein in both HeLa and HepG2 cells (*right* graphs of Fig. 4, *A* and *C*), with reduced glucose uptake (*left* graphs of Fig. 4, *B* and *D*). The altered transport activities of glucose caused by 4F2hc overexpression or siRNA treatment are generally very similar to those of leucine (*right* graphs of Fig. 3, *B* and *C*, and Fig. 4, *B* and *D*). To exclude the possibility of off-target effects of the siRNA knockdown experiments, we reintroduced a siRNA-resistant version of 4F2hc (siRNA is human; overexpressed 4F2hc is mouse). Reconstitution of mouse 4F2hc reversed the siRNA-mediated GLUT1 reduction (Supplemental Fig. S1*A*; Supplemental Material for this article is available online at the Journal website). In contrast, suppression of 4F2hc did not affect the expression of insulin Rβ (Supplemental Fig. S1*B*).

Enhanced green fluorescent protein (EGFP)-conjugated GLUT1 ligand, which has a receptor-binding domain in common with human T cell leukemia virus envelope glycoprotein, allows the amount of GLUT1 localized at the plasma membrane to be monitored by fluorescence staining (23, 24). Using this EGFP-conjugated ligand, we assessed the GLUT1 amount at the plasma membrane under conditions of either 4F2hc overexpression or knockdown in HeLa cells. The siRNA-mediated gene silencing of 4F2hc resulted in a reduction of the cell surface GLUT1 expression level, while 4F2hc overexpression produced an increase (Fig. 4*E*).

4F2hc is involved in GLUT1 stabilization and prevents GLUT1 from undergoing lysosomal degradation. To explore the mechanism underlying 4F2hc-related alterations in GLUT1 expression, we examined the mRNA levels of GLUT1 at 24 h and 48 h after the initiation of 4F2hc overexpression or 4F2hc siRNA transfection. Neither overexpression nor knockdown of 4F2hc significantly affected the mRNA levels of GLUT1 (Fig. 5, *A* and *B*). Since these observations indicate that 4F2hc does not regulate the transcriptional level of GLUT1, we considered the possibility that 4F2hc enhances GLUT1 stability and thereby increases glucose transport activity.

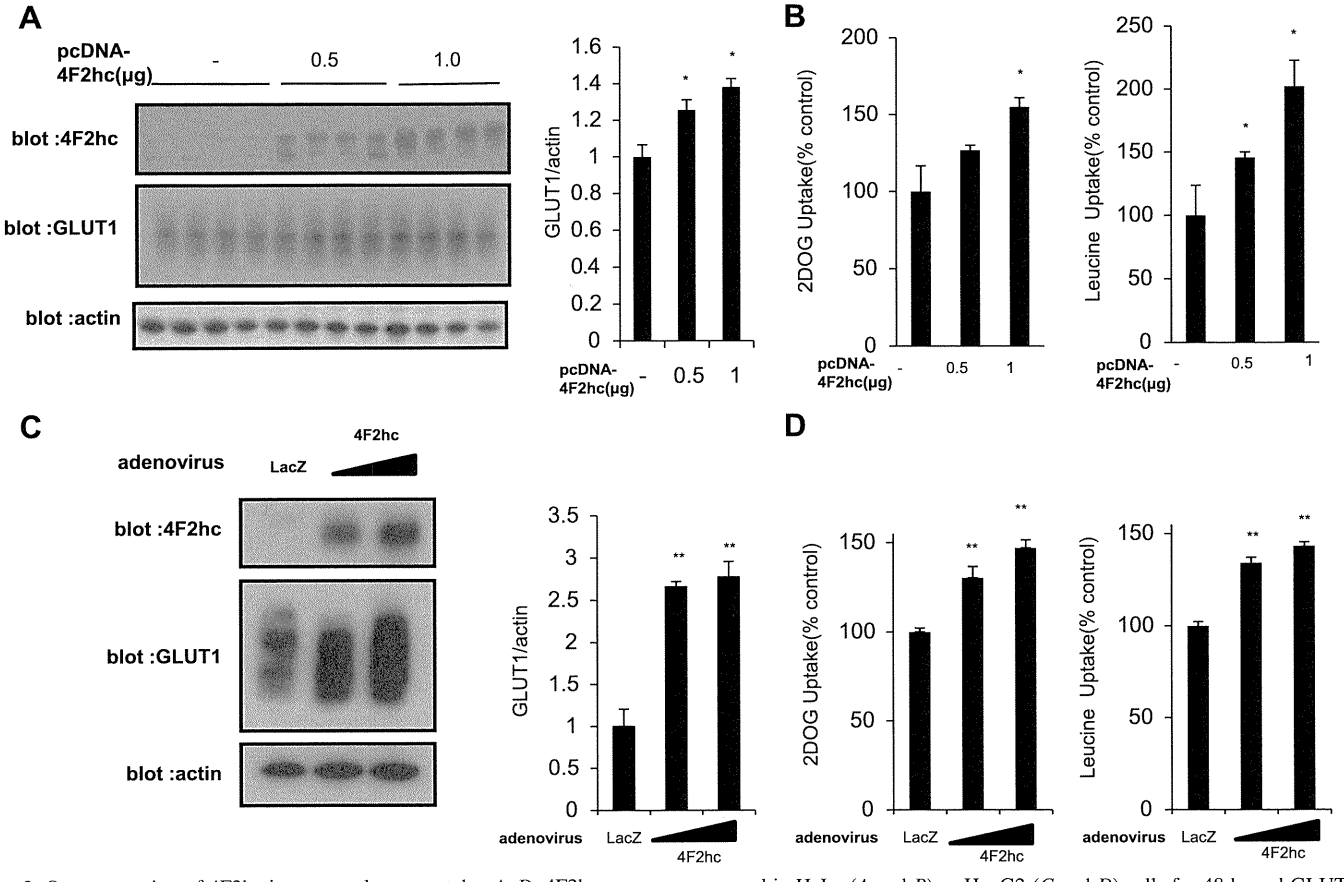

Fig. 3. Overexpression of 4F2hc increases glucose uptake. *A–D*: 4F2hc was overexpressed in HeLa (*A* and *B*) or HepG2 (*C* and *D*) cells for 48 h, and GLUT1 expression levels were measured by Western blotting and quantified (*A* and *C*). HepG2 cells were infected with LacZ adenovirus [50 multiplicity of infection (MOI)] or 4F2hc adenovirus (50 or 100 MOI). The uptakes of ^{3}H-2-deoxyglucose (2DOG; 5 min) and ^{14}C-leucine (1 min) were also measured (*B* and *D*). Data are expressed as means ± SE (n = 4). *P < 0.05; **P < 0.01, compared with controls.

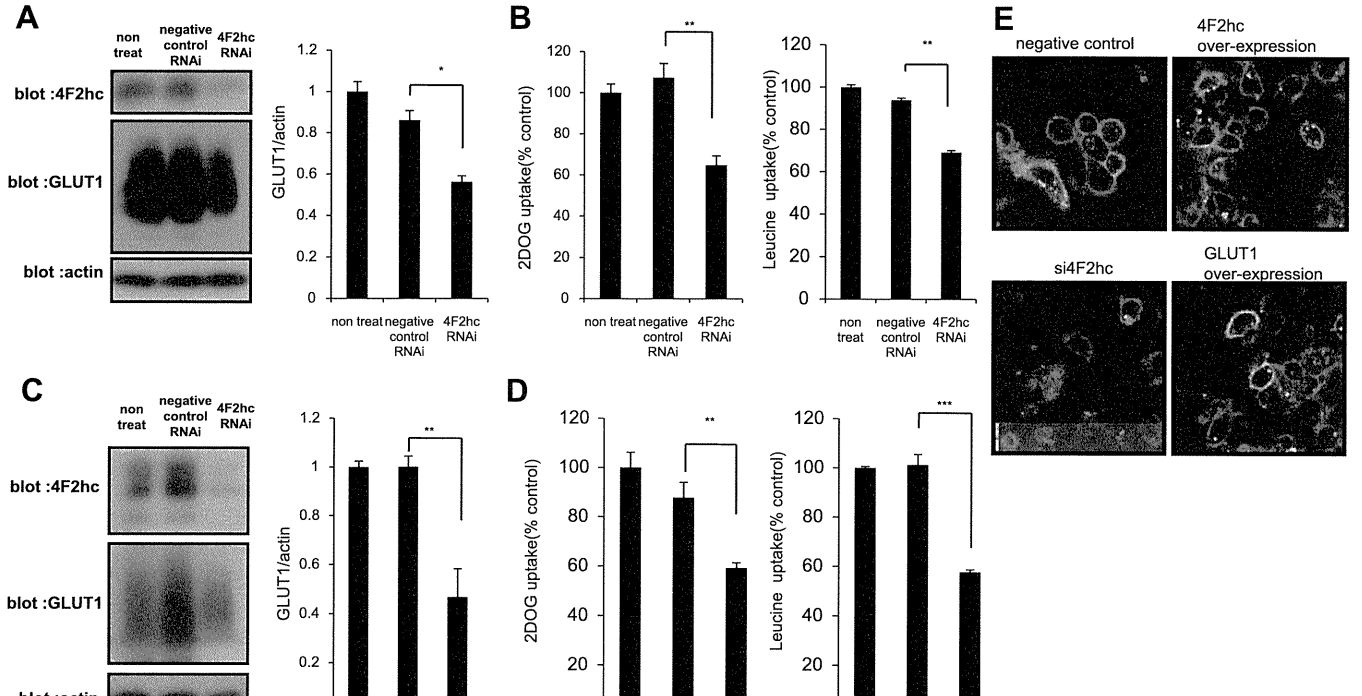

Fig. 4. Gene suppression of 4F2hc decreases glucose uptake. *A–D*: 4F2hc was suppressed in HeLa (*A* and *B*) and HepG2 (*C* and *D*) cells for 48 h, and GLUT1 expression levels were measured by Western blotting and quantified (*A* and *C*). The uptakes of ^{3}H-2-deoxyglucose (5 min) and ^{14}C-leucine (1 min) were also measured (*B* and *D*). *E*: 4F2hc or GLUT1 was overexpressed or small interfering RNA against 4F2hc (si4F2hc) was transfected into HeLa cells for 24 h. Enhanced GFP (EGFP)-conjugated GLUT1 ligand (AbCys, Paris, France) was added, and after a 30-min incubation, cell surface GLUT1 was observed by fluorescent microscopy. RNAi, RNA interference. Data are expressed as means ± SE (n = 4). *P < 0.05; **P < 0.01; ***P < 0.001, compared with negative controls.

The mechanism by which GLUT1 is degraded has not been elucidated in detail, but it has been shown that the lysosomal pathway contributes to GLUT1 degradation (30). GLUT1 degradation was investigated at the indicated period after addition of cycloheximide, an inhibitor of protein synthesis. Overexpression of 4F2hc significantly suppressed the GLUT1 degradation rate (Fig. 5*C*). On the other hand, the siRNA-mediated reduction in 4F2hc markedly increased the GLUT1 degradation rate, as compared with treatment with control siRNA (Fig. 5*D*). As previously reported, GLUT1 degradation was confirmed to be abolished by chloroquine, an agent suppressing lysosomal degradation (Fig. 5*E*) (32). In fact, it was shown that the proteasome blocker MG-132 did not stabilize GLUT1, which is consistent with previous reports (32). Taken together, our results strongly suggest that 4F2hc stabilizes GLUT1 by protecting it from lysosomal degradation.

DISCUSSION

In the present study, we newly demonstrated 4F2hc to be a protein interacting with GLUT1. 4F2hc, a membrane protein consisting of 529 amino acids and containing a single membrane-spanning domain, was initially identified as a lymphocyte activation antigen (13). 4F2hc reportedly forms a heterodimeric complex with specific light chain subunits of amino acid transporters such as LAT1 and LAT2 (14, 31, 33, 35). The heterodimer consisting of LAT1 or LAT2 and 4F2hc moves to the cell surface and exerts both neutral and basic amino acid transporter activity (25, 27). A previous study using deletion mutants revealed the domain of LAT1 indispensable for the association with 4F2hc to be the most NH_2-terminal transmembrane domain, and that a disulfide bridge connects their extracellular domains (5). A similar structure has been reported for the lactate transporter, which consists of 12 membrane-spanning monocarboxylate transporter 1 (MCT1) or MCT4 and a single membrane-spanning CD147 (20).

Given that GLUT1 has a similar structure, i.e., 12 putative membrane-spanning domains, similar to those of LAT1/2 and MCT1/4, we considered an association of 4F2hc with GLUT1 to be likely. We thus carried out experiments to assess this possibility. Indeed, the association between GLUT1 and 4F2hc was confirmed not only by coimmunoprecipitation of the overexpressed proteins, but also endogenously in HeLa cells and mouse brain, although it is unclear what percentage of GLUT1 is present as a heterodimer form with 4F2hc. While 4F2hc has a disulfide bridge between LAT1 with a cysteine on the extracellular side immediately after the transmembrane domain (5), this cysteine residue is not conserved in GLUT1, indicating that the association between GLUT1 and 4F2hc is not mediated by such a disulfide bond, but rather is simply noncovalent. Since the disulfide bridge connecting the extracellular domains of LAT1/2 and 4F2hc is not reportedly essential for association, the association between GLUT1 and 4F2hc without a disulfide bridge is not surprising (6, 27). However, in contrast to the essential role of 4F2hc in LAT1 or

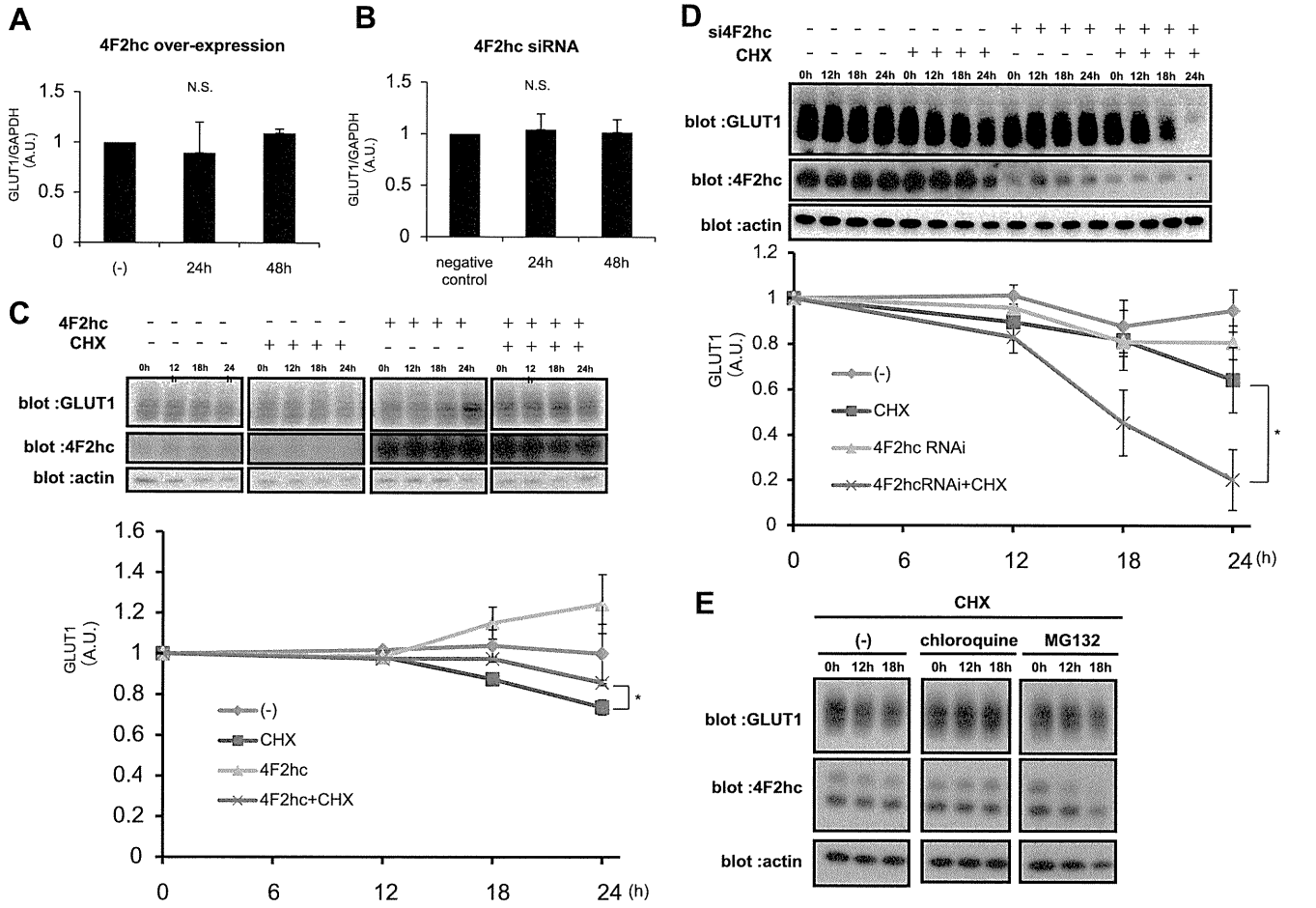

Fig. 5. 4F2hc is involved in GLUT1 stabilization and protects GLUT1 from lysosomal degradation. *A* and *B*: 4F2hc was overexpressed (*A*) or suppressed (*B*) in HeLa cells, and GLUT1 mRNA levels were measured by the real-time PCR method, at the indicated time (n = 6). NS, not significant; AU, arbitrary units. *C* and *D*: 4F2hc was overexpressed in HeLa cells (*C*) or suppressed in HepG2 cells (*D*) for 24 h. Then, cycloheximide (CHX) was added and the GLUT1 expression level was measured by Western blotting, at the indicated time. Graphs at *bottom* show GLUT1 level, expressed as the percentage of that at 0-h. *$P <$ 0.05 relative to cells with only CHX. *E*: 4F2hc was overexpressed in HeLa cells for 24 h. Then, CHX was added and GLUT1 degradation was observed in the presence of chloroquine or MG-132. Representative data from five independent experiments are shown.

LAT2 transport activity, GLUT1 can transport D-glucose without forming a complex with 4F2hc, an observation supported by previous reports showing the reconstitution of purified GLUT1 to an artificially constructed lectin membrane, as well as GLUT1 overexpression experiments in oocytes (15, 16, 17). Although we can speculate that heterodimeric complex formation with 4F2hc affects the kinetics of GLUT1 glucose transport activity to some degree, we were not able to clarify this issue herein because of difficulty measuring the percentages of GLUT1 alone and GLUT1/4F2hc forms.

On the other hand, it was clearly demonstrated that 4F2hc increases the amount of GLUT1 not only in whole cells but also at the plasma membrane. GLUT1 has been regarded as being involved in basal glucose uptake, and cells with high proliferative activity generally have high GLUT1 contents as shown in many cancers, fetal tissues, and the placenta (1, 22). We examined whether the 4F2hc expression level regulates not only amino acid transport activity via an association with LAT1, but also glucose transport activity via that with GLUT1. We found that 4F2hc overexpression increased not only leucine but also glucose uptake, while siRNA-mediated gene suppression of 4F2hc decreased these uptakes in HeLa and HepG2 cells (Figs. 3 and 4).

GLUT1 expression is elevated in highly proliferative cells. Oncogenes such as Ras and Src reportedly raise GLUT1 expression at the transcriptional level (4, 9). However, taking our results into consideration, the rate of GLUT1 degradation is also involved in regulation of the GLUT1 amount, and 4F2hc protects GLUT1 from lysosomal degradation. In addition, 4F2hc expression is also reportedly elevated in many cancers, suggesting its activity to correlate with cell proliferation and continuous growth (10, 19, 21, 28, 29). Thus, such growth-promoting stimuli not only increase GLUT1 synthesis at the transcriptional level, but also decrease the degradation of GLUT1 via upregulated 4F2hc. Previous reports described posttranscriptional modifications of GLUT1, such as monoubiquitinylation or sentrin conjugation, and their significance. These modifications reportedly regulate GLUT1 protein stability and cell function (7, 12). Thus, GLUT1 stability appears to also be important for determining both basal glucose uptake and cell proliferation. Taken together, these observations may support the hypothesis that increased expression of 4F2hc leads to an increased GLUT1 protein amount via suppression of GLUT1 degradation, resulting in the increased basal glucose uptake necessary for the progression of malignancy. In fact, the expression levels of both GLUT1 and 4F2hc are reportedly

elevated in many cancers and correlate with tumor progression (10, 28, 39). Further study is necessary to test our hypothesis.

In summary, our observations indicate that 4F2hc is likely to be involved in GLUT1 stabilization and to contribute to the regulation of not only amino acid but also glucose metabolism, both of which contribute to the incorporation of nutrients into highly proliferative cells. In this regard, the inhibition of 4F2hc may be regarded as a novel potential target for anticancer drugs.

ACKNOWLEDGMENTS

We thank Yoshikatsu Kanai for providing antibodies and the 3FLAG-4F2hc-expressing plasmid. This work was carried out with generous cooperation from the Research Center for Molecular Medicine, Hiroshima University.

DISCLOSURES

No conflicts of interest, financial or otherwise, are declared by the author(s).

REFERENCES

1. **Airley R, Mobasheri A.** Hypoxic regulation of glucose transport, anaerobic metabolism and angiogenesis in cancer: novel pathways and targets for anticancer therapeutics. *Chemotherapy* 53: 233–256, 2007.
2. **Asano T, Shibasaki Y, Ohno S, Taira H, Lin J, Kasuga M, Kanazawa Y, Akanuma Y, Takaku F, Oka Y.** Rabbit brain glucose transporter responds to insulin when expressed in insulin-sensitive Chinese hamster ovary cells. *J Biol Chem* 264: 3416–3420, 1989.
3. **Baer S, Casaubon L, Younes M.** Expression of the human erythrocyte glucose transporter Glut1 in cutaneous neoplasia. *J Am Acad Dermatol* 37: 575–577, 1997.
4. **Birnbaum M, Haspel H, Rosen O.** Transformation of rat fibroblasts by FSV rapidly increases glucose transporter gene transcription. *Science* 235: 1495–1498, 1987.
5. **Bröer S, Wagner C.** Structure-function relationships of heterodimeric amino acid transporters. *Cell Biochem Biophys* 36: 155–168, 2002.
6. **Fenczik C, Sethi T, Ramos J, Hughes P, Ginsberg M.** Complementation of dominant suppression implicates CD98 in integrin activation. *Nature* 390: 81–85, 1997.
7. **Fernandes R, Carvalho AL, Kumagai A, Seica R, Hosoya K, Terasaki T, Murta J, Pereira P, Faro C.** Downregulation of retinal GLUT1 in diabetes by ubiquitinylation. *Mol Vis* 10: 618–28, 2004.
8. **Fetchko M, Stagljar I.** Application of the split-ubiquitin membrane yeast two-hybrid system to investigate membrane protein interactions. *Methods* 32: 349–362, 2004.
9. **Flier J, Mueckler M, Usher P, Lodish H.** Elevated levels of glucose transport and transporter messenger RNA are induced by ras or src oncogenes. *Science* 235: 1492–1495, 1987.
10. **Fuchs B, Bode B.** Amino acid transporters ASCT2 and LAT1 in cancer: partners in crime? *Semin Cancer Biol* 15: 254–266, 2005.
11. **Ganapathy V, Thangaraju M, Prasad P.** Nutrient transporters in cancer: relevance to Warburg hypothesis and beyond. *Pharmacol Ther* 121: 29–40, 2009.
12. **Giorgino F, de Robertis O, Laviola L, Montrone C, Perrini S, McCowen KC, Smith RJ.** The sentrin-conjugating enzyme mUbc9 interacts with GLUT4 and GLUT1 glucose transporters and regulates transporter levels in skeletal muscle cells. *Proc Natl Acad Sci USA* 97: 1125–1130, 2000.
13. **Hemler M, Strominger J.** Characterization of antigen recognized by the monoclonal antibody (4F2): different molecular forms on human T and B lymphoblastoid cell lines. *J Immunol* 129: 623–628, 1982.
14. **Kanai Y, Segawa H, Miyamoto K, Uchino H, Takeda E, Endou H.** Expression cloning and characterization of a transporter for large neutral amino acids activated by the heavy chain of 4F2 antigen (CD98). *J Biol Chem* 273: 23629–23632, 1998.
15. **Kasahara M, Hinkle PC.** Reconstitution of D-glucose transport catalyzed by a protein fraction from human erythrocytes in sonicated liposomes. *Proc Natl Acad Sci USA* 73: 396–400, 1976.
16. **Kasahara M, Hinkle PC.** Reconstitution and purification of the D-glucose transporter from human erythrocytes. *J Biol Chem* 252: 7384–7390, 1977.
17. **Keller K, Strube M, Mueckler M.** Functional expression of the human HepG2 and rat adipocyte glucose transporters in *Xenopus* oocytes. Comparison of kinetic parameters. *J Biol Chem* 264: 18884–18889, 1989.
18. **Kim C, Cho S, Chun H, Lee S, Endou H, Kanai Y, Kim DK.** BCH, an inhibitor of system L amino acid transporters, induces apoptosis in cancer cells. *Biol Pharm Bull* 31: 1096–1100, 2008.
19. **Kim D, Kanai Y, Choi H, Tangtrongsup S, Chairoungdua A, Babu E, Tachampa K, Anzai N, Iribe Y, Endou H.** Characterization of the system L amino acid transporter in T24 human bladder carcinoma cells. *Biochim Biophys Acta* 1565: 112–121, 2002.
20. **Kirk P, Wilson M, Heddle C, Brown M, Barclay A, Halestrap A.** CD147 is tightly associated with lactate transporters MCT1 and MCT4 and facilitates their cell surface expression. *EMBO J* 19: 3896–3904, 2000.
21. **Kobayashi K, Ohnishi A, Promsuk J, Shimizu S, Kanai Y, Shiokawa Y, Nagane M.** Enhanced tumor growth elicited by L-type amino acid transporter 1 in human malignant glioma cells. *Neurosurgery* 62: 493–503, 2008.
22. **Macheda M, Rogers S, Best J.** Molecular and cellular regulation of glucose transporter (GLUT) proteins in cancer. *J Cell Physiol* 202: 654–662, 2005.
23. **Manel N, Battini J, Taylor N, Sitbon M.** HTLV-1 tropism and envelope receptor. *Oncogene* 24: 6016–6025, 2005.
24. **Manel N, Kim F, Kinet S, Taylor N, Sitbon M, Battini J.** The ubiquitous glucose transporter GLUT-1 is a receptor for HTLV. *Cell* 115: 449–459, 2003.
25. **Mastroberardino L, Spindler B, Pfeiffer R, Skelly P, Loffing J, Shoemaker C, Verrey F.** Amino-acid transport by heterodimers of 4F2hc/CD98 and members of a permease family. *Nature* 395: 288–291, 1998.
26. **Mueckler M, Caruso C, Baldwin S, Panico M, Blench I, Morris H, Allard W, Lienhard G, Lodish H.** Sequence and structure of a human glucose transporter. *Science* 229: 941–945, 1985.
27. **Nakamura E, Sato M, Yang H, Miyagawa F, Harasaki M, Tomita K, Matsuoka S, Noma A, Iwai K, Minato N.** 4F2 (CD98) heavy chain is associated covalently with an amino acid transporter and controls intracellular trafficking and membrane topology of 4F2 heterodimer. *J Biol Chem* 274: 3009–3016, 1999.
28. **Nawashiro H, Otani N, Shinomiya N, Fukui S, Nomura N, Yano A, Shima K, Matsuo H, Kanai Y.** The role of CD98 in astrocytic neoplasms. *Hum Cell* 15: 25–31, 2002.
29. **Ohkame H, Masuda H, Ishii Y, Kanai Y.** Expression of L-type amino acid transporter 1 (LAT1) and 4F2 heavy chain (4F2hc) in liver tumor lesions of rat models. *J Surg Oncol* 78: 265–271, 2001.
30. **Ortiz P, Honkanen R, Klingman D, Haspel H.** Regulation of the functional expression of hexose transporter GLUT-1 by glucose in murine fibroblasts: role of lysosomal degradation. *Biochemistry* 31: 5386–5393, 1992.
31. **Pineda M, Fernández E, Torrents D, Estévez R, López C, Camps M, Lloberas J, Zorzano A, Palacín M.** Identification of a membrane protein, LAT-2, that co-expresses with 4F2 heavy chain, an L-type amino acid transport activity with broad specificity for small and large zwitterionic amino acids. *J Biol Chem* 274: 19738–19744, 1999.
32. **Rosa SC, Gonçalves J, Judas F, Mobasheri A, Lopes C, Mendes AF.** Impaired glucose transporter-1 degradation and increased glucose transport and oxidative stress in response to high glucose in chondrocytes from osteoarthritic versus normal human cartilage. *Arthritis Res Ther* 11: R80, 2009.
33. **Rossier G, Meier C, Bauch C, Summa V, Sordat B, Verrey F, Kühn L.** LAT2, a new basolateral 4F2hc/CD98-associated amino acid transporter of kidney and intestine. *J Biol Chem* 274: 34948–34954, 1999.
34. **Sakoda H, Gotoh Y, Katagiri H, Kurokawa M, Ono H, Onishi Y, Anai M, Ogihara T, Fujishiro M, Fukushima Y, Abe M, Shojima N, Kikuchi M, Oka Y, Hirai H, Asano T.** Differing roles of Akt and serum- and glucocorticoid-regulated kinase in glucose metabolism, DNA synthesis, and oncogenic activity. *J Biol Chem* 278: 25802–25807, 2003.
35. **Segawa H, Fukasawa Y, Miyamoto K, Takeda E, Endou Kanai Y H.** Identification and functional characterization of a Na^+-independent neutral amino acid transporter with broad substrate selectivity. *J Biol Chem* 274: 19745–19751, 1999.
36. **Semenza G.** Targeting HIF-1 for cancer therapy. *Nat Rev Cancer* 3: 721–732, 2003.
37. **Smith T.** Facilitative glucose transporter expression in human cancer tissue. *Br J Biomed Sci* 56: 285–292, 1999.
38. **Stagljar I, Korostensky C, Johnsson N, te Heesen S.** A genetic system based on split-ubiquitin for the analysis of interactions between membrane proteins in vivo. *Proc Natl Acad Sci USA* 95: 5187–5192, 1998.
39. **Younes M, Brown RW, Stephenson M, Gondo M, Cagle PT.** Overexpression of Glut1 and Glut3 in stage I non-small cell lung carcinoma is associated with poor survival. *Cancer* 80: 1046–1051, 1997.

Hindawi Publishing Corporation
Experimental Diabetes Research
Volume 2011, Article ID 498460, 10 pages
doi:10.1155/2011/498460

Research Article

Frequent Loss of Genome Gap Region in 4p16.3 Subtelomere in Early-Onset Type 2 Diabetes Mellitus

Hirohito Kudo,[1] Mitsuru Emi,[2] Yasushi Ishigaki,[1] Uiko Tsunoda,[1] Yoshinori Hinokio,[1] Miho Ishii,[2] Hidenori Sato,[2] Tetsuya Yamada,[3] Hideki Katagiri,[3] and Yoshitomo Oka[1]

[1] *Division of Molecular Metabolism and Diabetes, Tohoku University Graduate School of Medicine, 2-1 Seiryo-machi, Aoba-ku, Sendai, Miyagi 980-8575, Japan*
[2] *CNV Laboratory, DNA Chip Research Institute, 1-1-43 Suehiro-cho, Tsurumi-ku Yokohama, Kanagawa 230-0045, Japan*
[3] *Department of Metabolic Diseases, Center for Metabolic Diseases, Tohoku University Graduate School of Medicine, 2-1 Seiryo-machi, Aoba-ku, Sendai, Miyagi 980-8575, Japan*

Correspondence should be addressed to Hideki Katagiri, katagiri@med.tohoku.ac.jp

Received 6 October 2010; Revised 21 February 2011; Accepted 30 March 2011

Academic Editor: Kazuya Yamagata

A small portion of Type 2 diabetes mellitus (T2DM) is familial, but the majority occurs as sporadic disease. Although causative genes are found in some rare forms, the genetic basis for sporadic T2DM is largely unknown. We searched for a copy number abnormality in 100 early-onset Japanese T2DM patients (onset age <35 years) by whole-genome screening with a copy number variation BeadChip. Within the 1.3-Mb subtelomeric region on chromosome 4p16.3, we found copy number losses in early-onset T2DM (13 of 100 T2DM versus one of 100 controls). This region surrounds a genome gap, which is rich in multiple low copy repeats. Subsequent region-targeted high-density custom-made oligonucleotide microarray experiments verified the copy number losses and delineated structural changes in the 1.3-Mb region. The results suggested that copy number losses of the genes in the deleted region around the genome gap in 4p16.3 may play significant roles in the etiology of T2DM.

1. Introduction

Type 2 diabetes mellitus (T2DM) is a common metabolic disease, affecting nearly 300 million individuals worldwide. T2DM affects over 10% of adult individuals over 40 years of age in Japan. The continuous increase in the number of patients is a major public health problem worldwide. Loci for rare monogenic forms of diabetes, such as maturity-onset diabetes of the young [1], mitochondrial diabetes [2, 3], and Wolfram syndrome [4], have been elucidated in a limited proportion of patients. However, the etiology of sporadic T2DM remains largely unknown. Accumulating epidemiological evidence [5–8] suggests that genetic factors play an important role in the susceptibility to sporadic T2DM, in addition to environmental factors such as obesity, aging, and exercise.

To search for susceptibility gene(s) for sporadic T2DM, genome-wide association studies (GWASs) using single nucleotide polymorphism (SNP) markers have been performed. These GWASs and replication studies have found multiple loci, *TCF7L2* [9], *KCNQ1* [10, 11], and others [12–18], that are associated with susceptibility to T2DM. However, the overall contribution of these SNPs to sporadic T2DM is relatively low; their odds ratio being in the range of 1.1–1.4 [9, 11]. In addition, these associations have not necessarily been replicated in subsequent studies [12–18].

Copy number variations (CNVs) or structural variations, such as deletion or gain of a genomic region, are increasingly recognized as important interindividual genetic variations across the human genome. CNVs account for more nucleotide variation between two individuals than do SNPs [19–21]. Repetitive, multicopy regions, such as segmental duplications and low copy repeats associated with CNV, are regarded as "rearrangement hotspots," and CNV regions are predisposed to the generation of deletion/duplication events [22]. Such repeat-rich regions were recently found to

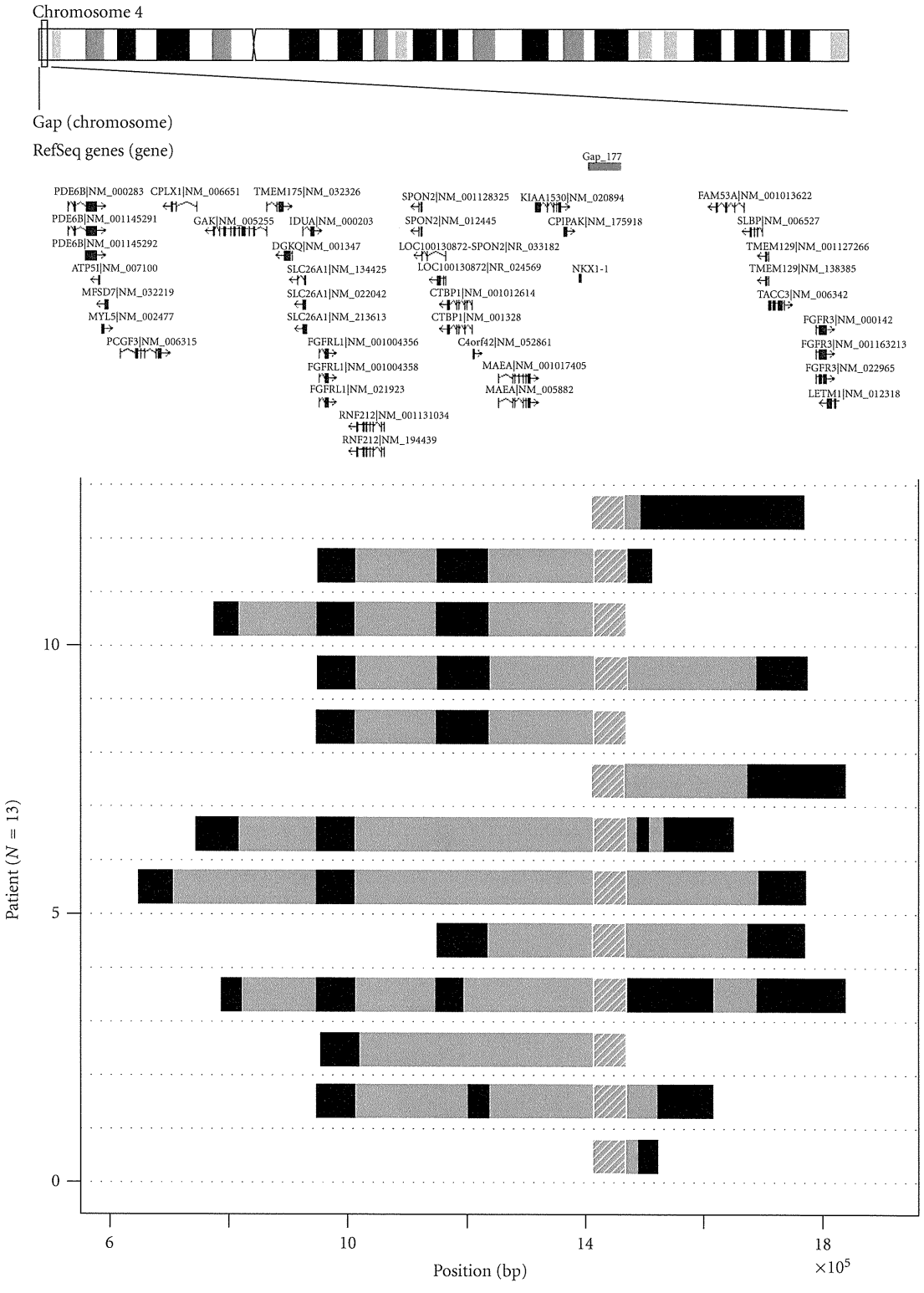

FIGURE 1: Genomic region harboring copy number loss of 1.3-Mb 4p16.3 subtelomeric region in 13 early-onset T2DM patients. Data measured by deCODE/Illumina CNV370K chip were analyzed by the PennCNV program. Genome structure of the 13 patients are aligned as horizontal bars from genome position 550,000 (left) to position 1,850,000 (right). Hatched region at position 1,423,147–1,478,646 represents genome gap-177 region. Dark solid horizontal bars represent extent of copy number loss in each T2DM patient. Gray regions between the dark bars represent intervals where copy number loss could not be inferred due to poor probe coverage. Upper map shows ideogram of chromosome 4 and the positions of putative genes in 4p16.3 region described in Database of Genomic Variants (http://projects.tcag.ca/variation/). Position is given relative to NCBI Build 35 for the chromosome 4.

show 13-fold enrichment of CNVs over the average genomic coverage in a reference assembly [23]. Therefore, CNVs or structural variations are recognized as significant contributors to human genetic disease and disease susceptibility [24].

In the search for susceptibility gene(s) for T2DM genes, we recruited a panel of 100 early-onset Japanese T2DM patients (onset age <35 years) and 100 controls, and performed CNV analysis in the whole genome using the deCODE-Illumina CNV370K BeadChip which focuses on the CNV-rich region of the human genome, followed by validation and characterization using an Agilent region-targeted high-density custom-made oligonucleotide tiling microarray. We found frequent copy number losses within the 1.3-Mb subtelomeric region in a substantial portion of early-onset Japanese T2DM patients. This region surrounds the genome gap in 4p16.3, which is rich in multiple low copy repeats.

2. Materials and Methods

2.1. Subjects. We considered that the early onset of T2DM reflects the presence of more genetic factors rather than environmental factors. Therefore, we adopted young-onset diabetic patients as case subjects. We studied 100 unrelated Japanese T2DM patients who developed T2DM before 35 years of age. They were recruited at Tohoku University Hospital and affiliated hospitals and medical clinics. Diabetes was diagnosed using the WHO criteria. Type 1 diabetes mellitus was excluded judged from clinical features and existence of anti-GAD (glutamic acid decarboxylase) antibodies or anti-IA-2 (insulinoma-associated antigen-2) antibodies. Patients with diabetes mellitus due to hepatic disease, pancreatic disease, other endocrinological disease, or mitochondrial DNA mutation, or drug-induced diabetes were excluded, judged from laboratory data and clinical history.

We also studied 100 nondiabetic control subjects, using the following criteria: 60 or more years of age, no prior diagnosis of diabetes mellitus, HbA1c less than 6.4% (where HbA1c (%) was estimated as an NGSP (National Glycohemoglobin Standardization Program) equivalent value (%) calculated by the formula HbA1c (%) = HbA1c (JDS: Japan Diabetes Society value) (%) + 0.4%, considering the relational expression of HbA1c (JDS) (%) measured by the previous Japanese standard substance and measurement methods for HbA1c (NGSP) [25] and no family history of T2DM within third-degree relatives, in order to exclude subjects who were more likely to develop diabetes later.

Clinical features available from 100 early-onset T2DM patients and 100 controls are shown in (see Table S1 in Supplementary Material available online at doi: 10.1155/2011/498460). In addition, clinical features of the 13 early-onset T2DM patients with copy number losses in 4p16.3 are shown separately in Supplementary Table S2 and Supplementary Table S3 in comparison with the rest of 100 early-onset T2DM patients without copy number loss ($n = 87$).

Genetic analysis of human subjects was approved by the ethics committee of Tohoku University Graduate School of Medicine. Appropriate informed consent was obtained from all the subjects examined.

2.2. Screening with Whole-Genome CNV BeadChip. We screened the whole genome by CNV analysis using the deCODE-Illumina CNV370K BeadChip (Illumina Infinium system, deCODE genetics, Inc., Iceland), which, in addition to Hap300 SNP marker contents, has CNV probes designed to target the CNV-rich region of the whole genome. The CNV part of the platform consists of probes covering CNV-rich regions of the genome, such as megasatellites (tandem repeats >500 bp), duplicons (region flanked by highly homologous segmental duplication >1 kb), unSNPable regions (>15 kb gaps in HapMap SNP map, and 5–15 kb gaps with >2SNPs with Hardy-Weinberg failure), and CNVs registered in the Database of Genomic Variants. The CNV part of probe content consists of 15,559 CNV segments covering 190 Mb, or 6% of the human genome. The platform has been tested in 4000 Icelandic and HapMap samples.

Data analysis of the deCODE-Illumina CNV chip was carried out using DosageMiner software developed by deCODE genetics, and loss/gain analysis consisted of the following four steps; (1) intensity normalization and GC content correction, (2) removal of batch effects using principal component analysis, (3) calling of clusters using a Gaussian mixture model, and (4) determination of CNV type using graphical constraints. In brief, CNVs were identified when CNV events stood out in the data, as all sample intensities for CNV probes should be increased or decreased relative to neighboring probes that are not in a CNV region. To determine deviations in signal intensity we started by normalizing the intensities. The normalized intensities for each color channel were determined by an equation and fit formula developed by deCODE genetics. A stretch with occurrence of more than one marker showing abnormality in the copy number in a consecutive stretch in the genome is considered more likely to be evidence of deletion or gain [26]. We display Supplementary Table to present raw data, that is, $\log_2$ ratio measured at each probe for every individual. Raw data at screening step via deCODE/Illumina beads chip for all probes on chromosome 4p is shown in Supplementary Table S4.

2.3. High-Density Custom-Made Oligonucleotide Tiling Microarray Analysis. DNA samples from 13 early-onset T2DM patients and 15 control individuals were subjected to Agilent's high-density custom-made oligonucleotide tiling microarray analysis based on an array comparative genomic hybridization (aCGH) assay. We fabricated a custom-designed microarray targeted to a 1.3-Mb genome region in the subtelomere at 4p16.3 (Chr. 4: 550,000-1,850,000 (NCBI Build 36.1, hg18)) according to previously described methods [27, 28]. In brief, we used the Agilent website (http://earray.chem.agilent.com/earray/) to select and design our custom tiling array; the array consisted of probes 60-mer in size (Agilent Technologies, Santa Clara, CA).

Tiling-aCGH experiments were performed essentially as described previously [29]. In brief, test and reference (NA19000, a Japanese male from HapMap project) genomic

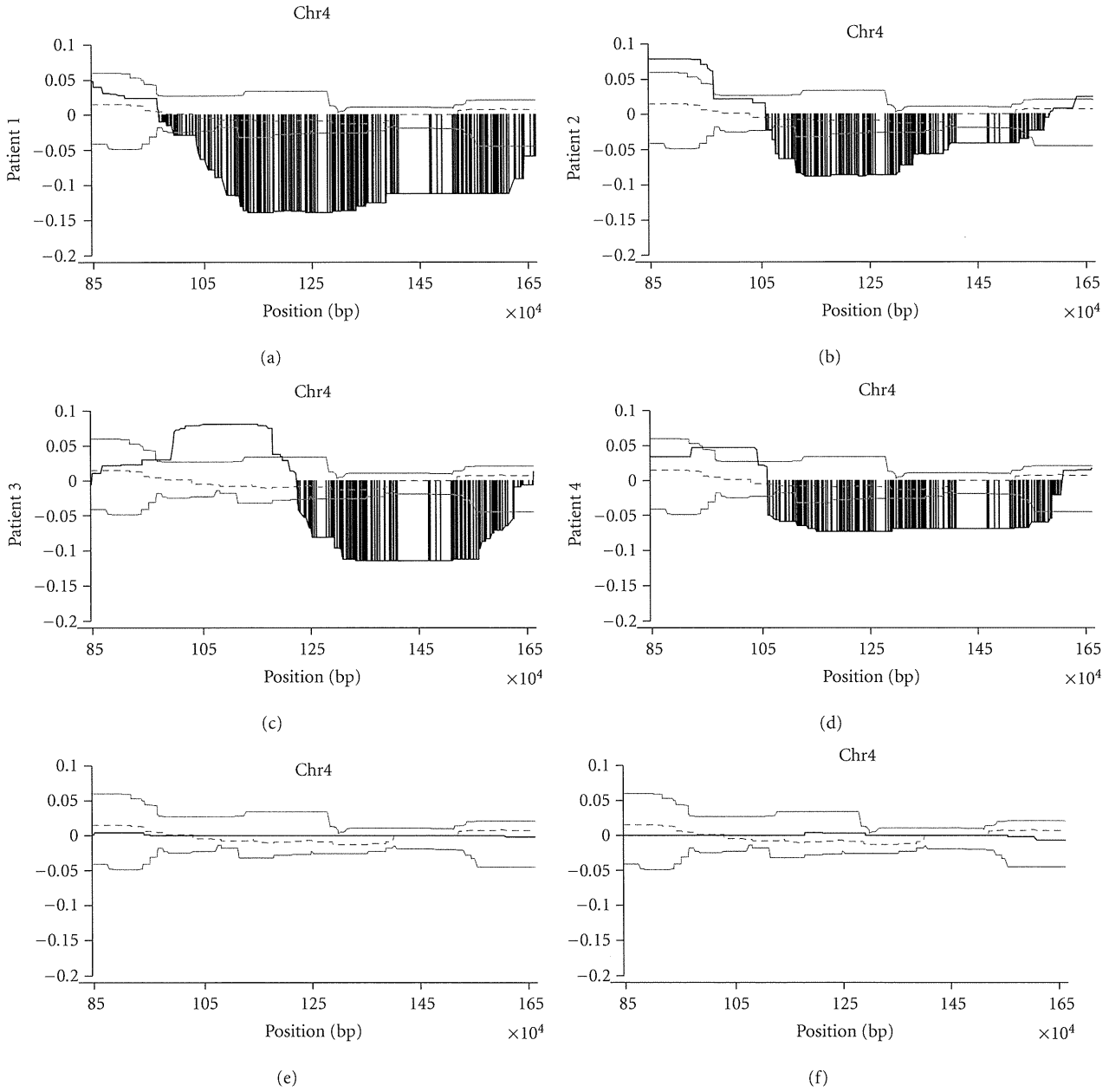

FIGURE 2: Detailed structure of copy number loss of 1.3-Mb 4p16.3 subtelomeric region resolved by high-density tiling microarray. Log_2 ratio (y-axis) was plotted using moving average along the genome position (x-axis). Four representative early-onset T2DM patients are shown as Figures 2(a), 2(b), 2(c), and 2(d), patient 1, 2, 3, and 4, respectively. For comparison, log_2 ratio of the region of two healthy normal individuals is also displayed as Figures 2(e) and 2(f). Dark line represents copy number plot along the genome. Two light lines indicate normal range of average log_2 ratios for probes among normal individuals. Dotted line shows median of average log_2 ratio among normal individuals. Copy number losses are displayed as gray vertical bar. We defined two copy number classes, that is, "unchanged copy number" and "copy number loss." "Unchanged copy number" was defined when the log_2 ratio stays within the mean ± 1 SD distribution among the normal population. "Copy number loss" was called when the downward-deviation of log_2 ratios exceeded a threshold of 1 SD from the median probe ratio.

DNAs (250 ng per sample) were fluorescently labeled with Cy5 (test) and Cy3 (reference) with a ULS Labeling Kit (Agilent Technologies).

For each sample, respective labeling reactions were mixed and then separated prior to hybridizing to each of the arrays. Labeled test and reference DNAs were combined, denatured, preannealed with Cot-1 DNA (Invitrogen) and blocking agent, and then hybridized to the arrays for 24 hr in a rotating oven at 65°C and 20 rpm (Agilent Technologies). After hybridization and washes, the arrays were scanned at 3 μm resolution with an Agilent G2505C scanner. Images were analyzed with Feature Extraction Software 10.7.3.1 (Agilent Technologies), with the CGH_107_Sep09 protocol for background subtraction and normalization. Detection

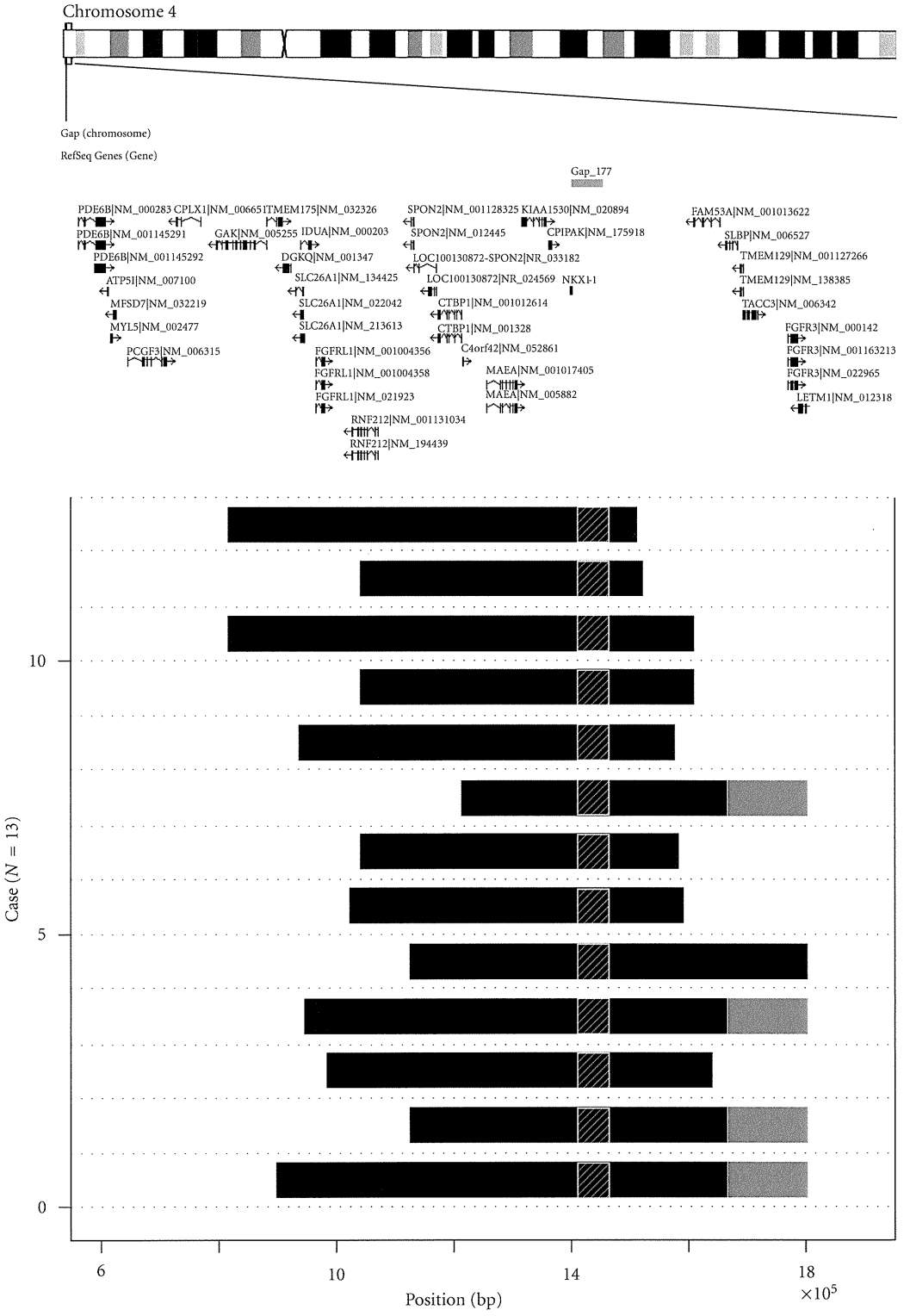

FIGURE 3: The extent of copy number losses within 1.3-Mb 4p16.3 subtelomeric region in 13 early-onset T2DM patients revealed by high-density oligonucleotide tiling microarray. Dark horizontal bars represent extent of copy number loss region in each patient revealed by Agilent custom tiling array. Genome structure of the 13 patients is aligned as horizontal bars from genome position 550,000 (left) to position 1,850,000 (right). Hatched region at position 1,423,147–1,478,646 represents genome gap-177 region. Gray regions represent proximal ends of stretch where copy number status was not inferred due to presence of multiple low copy repeats. Upper map shows ideogram of chromosome 4 and the positions of putative genes in 4p16.3 region described in Database of Genomic Variants (http://projects.tcag.ca/variation/). Position is given relative to NCBI Build 35 for the chromosome 4.

of abnormal copy number, losses, and gains, in a complex multicopy variable region by high-density tiling array was accessed by deviation of probe $\log_2$ ratios that exceeded a threshold of 1 SD from the median probe ratio, according to procedures described previously [29–31]. We defined two copy number classes, that is, "unchanged copy number" and "copy number loss." "Unchanged copy number" was defined when the $\log_2$ ratio stays within the mean ± 1 SD distribution among the normal population. "Copy number loss" was called when the downward-deviation of $\log_2$ ratios exceeded a threshold of 1 SD from the median probe ratio. Raw data, that is, $\log_2$ratio measured at each probe for every individual obtained by high-density custom-made tilling array analysis is shown in Supplementary Table S5.

3. Results

In searching for CNVs associated with early-onset T2DM, we screened the whole genome by CNV analysis using the deCODE-Illumina CNV370K BeadChip in 100 early-onset Japanese T2DM patients and 100 controls. We found four CNVs that fulfilled our screening criteria: (1) reliable CNV (size over 50-Kb, consisting of over 50 consecutive probes), (2) the association being statistically significant by Fisher's exact test which was accompanied by Bonferroni's correction. Four candidate CNV that fulfilled the criteria; that is, CNV on 4p16.3 ($P = 6.75 \times 10^{-3}$ by Fisher's exact test, $P < .05$ after Bonferroni's correction), CNV on 16p13.3 ($P = 3.44 \times 10^{-4}$ by Fisher's exact test, $P < .05$ after Bonferroni's correction), CNV on 16q24.3 ($P = 9.65 \times 10^{-3}$ by Fisher's exact test, $P < .05$ after Bonferroni's correction), and CNV on 19p 13.3 ($P = 1.61 \times 10^{-4}$ by Fisher's exact test, $P < .05$ after Bonferroni's correction). Of these CNVs listed, the CNV on 4p16.3 was intriguingly found to be located right on the genome gap-177 region on 4p subtelomere. At this candidate CNV on 4p16.3, 13 out of 100 T2DM patients displayed CN-loss around this CNV marker, compared with 1 out of 100 control samples. Because of its unique overlap with genome gap structure, we focused on this CNV region for further analysis.

Figure 1 shows the pattern of alterations in copy number loss observed among the 100 early-onset Japanese 2DM patients. Thirteen patients displayed copy number losses around the gap in the 4p16.3 subtelomere whereas only one of 100 control samples showed copy number losses in this region. The association was statistically significant by Fisher's exact test ($P = 6.75 \times 10^{-3}$, OR = 14.7, 95% confidence interval 3.02–72.3). We observed two copy number classes, that is, "unchanged copy number" and "copy number loss" at 1.3-Mb region of chromosome 4p16.3 in our diabetic or control populations. The latter was found frequently observed among early-onset T2DM patients at the 4p16.3 subtelomere. The position, length, or pattern of deletion between one copy number loss in control and 13 copy number losses in T2DM patients were not apparently distinct, although the case number is too small to draw meaningful conclusion.

To verify the CNV BeadChip results, we analyzed copy number changes along the 1.3-Mb region in the subtelomere surrounding the genome gap of 4p16.3 using a high-density custom-made oligonucleotide tiling microarray. We used peripheral blood DNA of the 13 early-onset T2DM patients, identified, and 15 control healthy individuals. Again, we found frequent copy number losses in regions around the genome gap in all the 13 early-onset T2DM patients, whereas none of 15 healthy individuals showed copy number losses.

Figure 2 shows detailed structure of copy number losses in four representative early-onset Japanese T2DM patients with copy number losses, in the 1.3-Mb region in the subtelomere (patients 1, 2, 3, 4; in Figures 2(a), 2(b), 2(c), and 2(d), resp.). Individual copy number plots using moving average (y-axis) versus distance along the chromosome (x-axis) are shown. As a comparison, copy number plots of healthy individuals who did not exhibit copy number alterations in the region are also shown (Figures 2(e) and 2(f)).

Figure 3 shows genomic copy number losses in all the 13 early-onset T2DM patients. High-density tiling custom-made microarray showed segmental losses in the subtelomeric region of 4p16.3 in all the 13 patients. Genomic copy number losses in these patients were clustered around a gap region in the 4p16.3 subtelomeric region.

4. Discussion

Our initial genome-wide screening with deCODE-Illumina CNV370K BeadChip for association with early-onset T2DM revealed losses in the subtelomeric region of 4p16.3. Subsequent high-density custom-made oligonucleotide tiling microarray verified copy number losses in this region.

It is worthy to note that most patients with copy number losses were treated with insulin injection. Urine C-peptide reactivity was not significantly different between the two groups, and only few patients underwent glucagon challenge test, thus, the data are too limited to infer the function of insulin secretion. We did not observe significant differences between two groups as to age of onset, body mass index, postprandial plasma glucose levels, or HbA1c levels. Fasting immunoreactive insulin levels were examined in 5 patients with copy number losses and 14 patients without copy number loss. HOMA-R in the former patients was 6.1 ± 6.8 (mean ± SD) and that in the latter patients was 5.5 ± 6.0 (mean ± SD); these values were not significantly different. Incidence of dyslipidemia, hypertension, diabetic retinopathy, nephropathy, or neuropathy was not different between the two groups (Supplementary Tables S2, S3). Further investigation of a large panel of patients would be necessary to clarify any clinical differences that might be present between the two groups.

The current map of CNV in the human genome reported in the existing databases is far from complete [32]. Increasing numbers of CNVs have recently been identified around repetitive sequences such as segmental duplications or low copy repeats. In fact, these repeat-rich regions were found to be 13-fold enriched in CNV over the average genomic coverage in the reference assembly [23]. Probes for conventional genome-wide SNP genotyping platforms are likely to be underrepresented; that is, only 25% and 40% of CNV are

Table 1: Putative genes located within 1.3-Mb region in 4p16.3 subtelomere.

Start	End	Cytogenetic location	Symbol	Description	Model evidence
609,373	654,571	4p16.3	PDE6B	Phosphodiesterase 6B, cGMP-specific, rod, beta (congenital stationary night blindness 3, autosomal dominant)	Best RefSeq
656,225	658,122	4p16.3	ATP5I	ATP synthase, H+ transporting, mitochondrial F0 complex, subunit E	Best RefSeq
661,711	665,817	4p16.3	MYL5	Myosin, light chain 5, regulatory	Best RefSeq
665,618	672,973	4p16.3	MFSD7	Major facilitator superfamily domain containing 7	mRNA
689,573	754,428	4p16.3	PCGF3	Polycomb group ring finger 3	Best RefSeq
719,829	721,544	4p16.3	LOC100128084	Hypothetical protein LOC100128084	mRNA
764,588	765,632	4p16.3	LOC100129917	Hypothetical protein LOC100129917	mRNA
768,745	809,945	4p16.3	CPLX1	Complexin 1	mRNA
833,065	916,174	4p16.3	GAK	Cyclin G associated kinase	mRNA
916,262	942,444	4p16.3	TMEM175	Transmembrane protein 175	Best RefSeq
942,675	957,344	4p16.3	DGKQ	Diacylglycerol kinase, theta 110 kDa	Best RefSeq
962,861	977,224	4p16.3	SLC26A1	Solute carrier family 26 (sulfate transporter), member 1	Best RefSeq
970,785	988,317	4p16.3	IDUA	Iduronidase, alpha-L-	mRNA
995,610	1,010,686	4p16.3	FGFRL1	Fibroblast growth factor receptor-like 1	Best RefSeq
1,044,654	1,045,386	4p16.3	LOC100132787	Hypothetical protein LOC100132787	mRNA
1,055,269	1,097,350	4p16.3	RNF212	Ring finger protein 212	Best RefSeq
1,116,050	1,129,814	4p16.3	LOC100133135	Hypothetical protein LOC100133135	Protein
1,135,541	1,135,957	4p16.3	FLJ35816	FLJ35816 protein	Protein
1,149,293	1,149,712	4p16.3	LOC100131106	Hypothetical protein LOC100131106	Protein
1,150,723	1,156,597	4p16.3	SPON2	Spondin 2, extracellular matrix protein	Best RefSeq
1,184,431	1,185,198	4p16.3	LOC100130872	Hypothetical protein LOC100130872	mRNA
1,195,228	1,232,908	4p16.3	CTBP1	C-terminal binding protein 1	Best RefSeq
1,234,177	1,236,616	4p16.3	C4orf42	Chromosome 4 open reading frame 42	Best RefSeq
1,273,672	1,323,925	4p16.3	MAEA	Macrophage erythroblast attacher	Best RefSeq
1,331,104	1,371,732	4p16.3	KIAA1530	KIAA1530	mRNA
1,375,340	1,379,782	4p16.3	CRIPAK	Cysteine-rich PAK1 inhibitor	mRNA
1,380,072	1,392,453	4p16.3	NKX1-1	NK1 homeobox 1	Protein
1,484,196	1,519,086	4p16.3	LOC100133199	Similar to RE32881p	mRNA
1,611,605	1,655,516	4p16.3	FAM53A	Family with sequence similarity 53, member A	Best RefSeq
1,664,325	1,683,828	4p16.3	SLBP	Stem-loop (histone) binding protein	Best RefSeq
1,687,477	1,692,882	4p16.3	TMEM129	Transmembrane protein 129	Best RefSeq
1,693,062	1,716,696	4p16.3	TACC3	Transforming, acidic coiled-coil containing protein 3	Best RefSeq
1,765,421	1,780,396	4p16.3	FGFR3	Fibroblast growth factor receptor 3 (achondroplasia, thanatophoric dwarfism)	Best RefSeq
1,784,558	1,827,772	4p16.3	LETM1	Leucine zipper-EF-hand containing transmembrane protein 1	Best RefSeq

covered by the HumanHap300 and HumanHap550 platform, respectively [23]. These recent findings may partly explain why earlier genome-wide association studies for CNVs in the T2DM population failed to detect CNV loci being strongly associated with T2DM [20, 21, 33, 34].

We found copy number losses among early-onset Japanese T2DM patients in a region surrounding a genome gap (gap-177) in the subtelomere of chromosome 4p16.3. The physical map of the human genome still contains a significant number of genome gaps; over 300 gaps still remain in the human draft genome sequence [35] that are considered inaccessible by most existing genotyping and sequencing technologies [36]. These gap regions are estimated to harbor ~1000 genes, which comprise approximately 5% of

the human genome (~200 Mb). In particular, they are abundant in subtelomeres and pericentromeric regions of chromosomes [37, 38]. Some of these gaps are thought to be susceptible sites for mediating meiotic recombination and are also susceptibility sites for break points for deletions [39, 40].

Many CNVs were recently identified in repeat-rich regions [41], which are predisposed to the generation of deletion/duplication events [22]. It is intriguing to note that the locus-specific mutation rates for CNV or structural rearrangements were estimated to be between 10^{-6} and 10^{-4}: two to four orders of magnitude greater than nucleotide-specific rates for base substitutions or point mutations [19].

The deleted CNV region found in the present study and its flanking region contained 34 genes (Table 1). Gene(s) in this region may predispose to T2DM.

Genes involved in the glucose-induced insulin secretion cascade of pancreatic beta-cells are located in the region, such as ATP5I (ATP synthase, H^+ transporting, mitochondrial F_0 complex, subunit E) [42, 43], CPLX1 (complexin 1) [44, 45], GAK (cyclin G associated kinase) in association with CDK5 (cyclin-dependent protein kinases 5) [46–50], and CRIPAK (cysteine-rich PAK1 inhibitor), which is a negative regulator of PAK1 (p21 protein (Cdc42/Rac-) activated kinase 1) [51, 52].

FGFR3 (fibroblast growth factor receptor 3) and FGFRL1 (fibroblast growth factor receptor-like 1) are suggested to be involved in pancreatic development and differentiation [53–56]. TACC3 (transforming, acidic coiled-coil containing protein 3) may be involved in embryonic development including the pancreas [57, 58].

CTBP1 (C-terminal binding protein 1) and MAEA (macrophage erythroblast attacher) have effects on adipose tissue functions [59, 60], which may lead to insulin resistance. NKX1-1(NK1 homeobox 1) may cause insulin resistance with a function in the maintenance of energy homeostasis [61].

Recently, through whole-genome screening of a copy number variation using a CNV BeadChip and real-time quantitative polymerase chain reaction (qPCR), Kato et al. identified a segmental copy number gain within the 40-kb region on 10p15.3 subtelomere in patients of sporadic amyotrophic lateral sclerosis (SALS) [62]. They demonstrated the copy number gain in 46 out of 83 SALS patients, as compared with 10 out of 99 controls. The copy number gain region they identified is rather small (40-kb) and harbored two genes encoding isopentenyl diphosphate isomerase 1 (IDI1) and IDI2. Thus, they suggested the copy number gain in the region of these genes may play a significant role in the pathogenesis of SALS. The present study share a similar genome abnormality in that we found frequent copy number alterations in subtelomere region among sporadic adult-onset disease of unknown cause. The copy number alterations we identified here in early-onset T2DM were copy number losses on different chromosome subtelomere (4p16.3) and the size is rather large (up to 1.3-Mb). In our case, we suspect that multiple genes in the region may be involved in diabetes pathogenesis through impairments caused by copy number losses.

5. Conclusion

These results suggested that copy number losses of the candidate genes in the deleted region surrounding the genome gap in 4p16.3 may play significant roles in the etiology of T2DM. Further functional study, as well as investigation of 4p16.3 loss in a large panel of early-onset T2DM patients in different ethnic populations and geographical regions, is warranted.

Acknowledgment

This paper was supported by a Grant-in-Aid for Scientific Research to Y. Oka (H19-genome-005) from the Ministry of Health, Labor, and Welfare of Japan, and was also supported by a grant from the Global-COE Programs for "Network Medicine" to Y. Oka and H. Katagiri from the Ministry of Education, Culture, Sports, Science, and Technology of Japan.

References

[1] T. M. Frayling, J. C. Evans, M. P. Bulman et al., "beta-cell genes and diabetes: molecular and clinical characterization of mutations in transcription factors," *Diabetes*, vol. 50, supplement 1, pp. S94–S100, 2001.

[2] J. M. van den Ouweland, H. H. Lemkes, W. Ruitenbeek et al., "Mutation in mitochondrial tRNA(Leu)(UUR) gene in a large pedigree with maternally transmitted type II diabetes mellitus and deafness," *Nature Genetics*, vol. 1, no. 5, pp. 368–371, 1992.

[3] Y. Oka, H. Katagiri, Y. Yazaki, T. Murase, and T. Kobayashi, "Mitochondrial gene mutation in islet-cell-antibody-positive patients who were initially non-insulin-dependent diabetics," *The Lancet*, vol. 342, no. 8870, pp. 527–528, 1993.

[4] H. Inoue, Y. Tanizawa, J. Wasson et al., "A gene encoding a transmembrane protein is mutated in patients with diabetes mellitus and optic atrophy (Wolfram syndrome)," *Nature Genetics*, vol. 20, no. 2, pp. 143–148, 1998.

[5] J. Kaprio, J. Tuomilehto, M. Koskenvuo et al., "Concordance for Type 1 (insulin-dependent) and Type 2 (non-insulin-dependent) diabetes mellitus in a population-based cohort of twins in Finland," *Diabetologia*, vol. 35, no. 11, pp. 1060–1067, 1992.

[6] P. Poulsen, K. O. Kyvik, A. Vaag, and H. Beck-Nielsen, "Heritability of type II (non-insulin-dependent) diabetes mellitus and abnormal glucose tolerance—a population-based twin study," *Diabetologia*, vol. 42, no. 2, pp. 139–145, 1999.

[7] J. B. Meigs, L. A. Cupples, and P. W. Wilson, "Parental transmission of type 2 diabetes: the Framingham Offspring Study," *Diabetes*, vol. 49, no. 12, pp. 2201–2207, 2000.

[8] C. F. Weijnen, S. S. Rich, J. B. Meigs, A. S. Krolewski, and J. H. Warram, "Risk of diabetes in siblings of index cases with Type 2 diabetes: implications for genetic studies," *Diabetic Medicine*, vol. 19, no. 1, pp. 41–50, 2002.

[9] S. F. Grant, G. Thorleifsson, I. Reynisdottir et al., "Variant of transcription factor 7-like 2 (TCF7L2) gene confers risk of type 2 diabetes," *Nature Genetics*, vol. 38, no. 3, pp. 320–323, 2006.

[10] H. Unoki, A. Takahashi, T. Kawaguchi et al., "SNPs in KCNQ1 are associated with susceptibility to type 2 diabetes in East Asian and European populations," *Nature Genetics*, vol. 40, no. 9, pp. 1098–1102, 2008.

[11] K. Yasuda, K. Miyake, Y. Horikawa et al., "Variants in KCNQ1 are associated with susceptibility to type 2 diabetes mellitus," *Nature Genetics*, vol. 40, no. 9, pp. 1092–1097, 2008.

[12] R. Saxena, B. F. Voight, V. Lyssenko et al., "Genome-wide association analysis identifies loci for type 2 diabetes and triglyceride levels," *Science*, vol. 316, no. 5829, pp. 1331–1336, 2007.

[13] L. J. Scott, K. L. Mohlke, L. L. Bonnycastle et al., "A genome-wide association study of type 2 diabetes in Finns detects multiple susceptibility variants," *Science*, vol. 316, no. 5829, pp. 1341–1345, 2007.

[14] R. Sladek, G. Rocheleau, J. Rung et al., "A genome-wide association study identifies novel risk loci for type 2 diabetes," *Nature*, vol. 445, no. 7130, pp. 881–885, 2007.

[15] V. Steinthorsdottir, G. Thorleifsson, I. Reynisdottir et al., "A variant in CDKAL1 influences insulin response and risk of type 2 diabetes," *Nature Genetics*, vol. 39, no. 6, pp. 770–775, 2007.

[16] E. Zeggini, M. N. Weedon, C. M. Lindgren et al., "Replication of genome-wide association signals in UK samples reveals risk loci for type 2 diabetes," *Science*, vol. 316, no. 5829, pp. 1336–1341, 2007.

[17] I. Prokopenko, M. I. McCarthy, and C. M. Lindgren, "Type 2 diabetes: new genes, new understanding," *Trends in Genetics*, vol. 24, no. 12, pp. 613–621, 2008.

[18] E. Zeggini, L. J. Scott, R. Saxena et al., "Meta-analysis of genome-wide association data and large-scale replication identifies additional susceptibility loci for type 2 diabetes," *Nature Genetics*, vol. 40, no. 5, pp. 638–645, 2008.

[19] J. R. Lupski, "Genomic rearrangements and sporadic disease," *Nature Genetics*, vol. 39, no. 7s, pp. S43–S47, 2007.

[20] D. F. Conrad, D. Pinto, R. Redon et al., "Origins and functional impact of copy number variation in the human genome," *Nature*, vol. 464, no. 7289, pp. 704–712, 2010.

[21] H. Park, J. I. Kim, Y. S. Ju et al., "Discovery of common Asian copy number variants using integrated high-resolution array CGH and massively parallel DNA sequencing," *Nature Genetics*, vol. 42, no. 5, pp. 400–405, 2010.

[22] A. J. Sharp, D. P. Locke, S. D. McGrath et al., "Segmental duplications and copy-number variation in the human genome," *American Journal of Human Genetics*, vol. 77, no. 1, pp. 78–88, 2005.

[23] G. M. Cooper, T. Zerr, J. M. Kidd, E. E. Eichler, and D. A. Nickerson, "Systematic assessment of copy number variant detection via genome-wide SNP genotyping," *Nature Genetics*, vol. 40, no. 10, pp. 1199–1203, 2008.

[24] R. Redon, S. Ishikawa, K. R. Fitch et al., "Global variation in copy number in the human genome," *Nature*, vol. 444, no. 7118, pp. 444–454, 2006.

[25] Y. Seino, K. Nanjo, N. Tajima et al., "Report of the committee on the classification and diagnostic criteria of diabetes mellitus," *Journal of the Japan Diabetes Society*, vol. 53, no. 6, pp. 450–467, 2010.

[26] H. Stefansson, D. Rujescu, S. Cichon et al., "Large recurrent microdeletions associated with schizophrenia," *Nature*, vol. 455, no. 7210, pp. 232–236, 2008.

[27] M. T. Barrett, A. Scheffer, A. Ben-Dor et al., "Comparative genomic hybridization using oligonucleotide microarrays and total genomic DNA," *Proceedings of the National Academy of Sciences of the United States of America*, vol. 101, no. 51, pp. 17765–17770, 2004.

[28] G. H. Perry, A. Ben-Dor, A. Tsalenko et al., "The fine-scale and complex architecture of human copy-number variation," *American Journal of Human Genetics*, vol. 82, no. 3, pp. 685–695, 2008.

[29] A. J. de Smith, A. Tsalenko, N. Sampas et al., "Array CGH analysis of copy number variation identifies 1284 new genes variant in healthy white males: implications for association studies of complex diseases," *Human Molecular Genetics*, vol. 16, no. 23, pp. 2783–2794, 2007.

[30] A. J. Sharp, S. Hansen, R. R. Selzer et al., "Discovery of previously unidentified genomic disorders from the duplication architecture of the human genome," *Nature Genetics*, vol. 38, no. 9, pp. 1038–1042, 2006.

[31] J. R. Lupski, "Genomic disorders ten years on," *Genome Medicine*, vol. 1, no. 4, p. 42, 2009.

[32] I. Ionita-Laza, A. J. Rogers, C. Lange, B. A. Raby, and C. Lee, "Genetic association analysis of copy-number variation (CNV) in human disease pathogenesis," *Genomics*, vol. 93, no. 1, pp. 22–26, 2009.

[33] C. Shtir, R. Pique-Regi, K. Siegmund, J. Morrison, F. Schumacher, and P. Marjoram, "Copy number variation in the Framingham Heart Study," *BioMed Central Proceedings*, vol. 3, supplement 7, p. S133, 2009.

[34] The Wellcome Trust Case Control Consortium, "Genome-wide association study of CNVs in 16,000 cases of eight common diseases and 3,000 shared controls," *Nature*, vol. 464, no. 7289, pp. 713–720, 2010.

[35] International Human Genome Sequencing Consortium, "Finishing the euchromatic sequence of the human genome," *Nature*, vol. 431, no. 7011, pp. 931–945, 2004.

[36] E. E. Eichler, J. Flint, G. Gibson et al., "Missing heritability and strategies for finding the underlying causes of complex disease," *Nature Reviews Genetics*, vol. 11, no. 6, pp. 446–450, 2010.

[37] C. M. Lese, J. A. Fantes, H. C. Riethman, and D. H. Ledbetter, "Characterization of physical gap sizes at human telomeres," *Genome Research*, vol. 9, no. 9, pp. 888–894, 1999.

[38] E. E. Eichler, R. A. Clark, and X. She, "An assessment of the sequence gaps: unfinished business in a finished human genome," *Nature Reviews Genetics*, vol. 5, no. 5, pp. 345–354, 2004.

[39] K. Devriendt and J. R. Vermeesch, "Chromosomal phenotypes and submicroscopic abnormalities," *Human genomics*, vol. 1, no. 2, pp. 126–133, 2004.

[40] G. Van Buggenhout, C. Melotte, B. Dutta et al., "Mild Wolf-Hirschhorn syndrome: micro-array CGH analysis of atypical 4p16.3 deletions enables refinement of the genotype-phenotype map," *Journal of Medical Genetics*, vol. 41, no. 9, pp. 691–698, 2004.

[41] A. Itsara, G. M. Cooper, C. Baker et al., "Population analysis of large copy number variants and hotspots of human genetic disease," *American Journal of Human Genetics*, vol. 84, no. 2, pp. 148–161, 2009.

[42] D. A. Swartz, E. I. Park, W. J. Visek, and J. Kaput, "The e subunit gene of murine FF-ATP synthase. Genomic sequence, chromosomal mapping, and diet regulation," *Journal of Biological Chemistry*, vol. 271, no. 34, pp. 20942–20948, 1996.

[43] T. Hayakawa, M. Noda, K. Yasuda et al., "Ethidium bromide-induced inhibition of mitochondrial gene transcription suppresses glucose-stimulated insulin release in the mouse pancreatic beta-cell cell line betaHC9," *Journal of Biological Chemistry*, vol. 273, no. 32, pp. 20300–20307, 1998.

[44] A. Abderrahmani, G. Niederhauser, V. Plaisance et al., "Complexin I regulates glucose-induced secretion in pancreatic beta-cells," *Journal of Cell Science*, vol. 117, no. 11, pp. 2239–2247, 2004.

[45] M. Dubois, P. Vacher, B. Roger et al., "Glucotoxicity inhibits late steps of insulin exocytosis," *Endocrinology*, vol. 148, no. 4, pp. 1605–1614, 2007.

[46] Y. Kanaoka, S. H. Kimura, I. Okazaki, M. Ikeda, and H. Nojima, "GAK: a cyclin G associated kinase contains a tensin/auxilin-like domain," *Federation of European Biochemical Societies Letters*, vol. 402, no. 1, pp. 73–80, 1997.

[47] S. H. Kimura, H. Tsuruga, N. Yabuta, Y. Endo, and H. Nojima, "Structure, expression, and chromosomal localization of human GAK," *Genomics*, vol. 44, no. 2, pp. 179–187, 1997.

[48] F. Y. Wei, K. Nagashima, T. Ohshima et al., "Cdk5-dependent regulation of glucose-stimulated insulin secretion," *Nature Medicine*, vol. 11, no. 10, pp. 1104–1108, 2005.

[49] M. Ubeda, J. M. Rukstalis, and J. F. Habener, "Inhibition of cyclin-dependent kinase 5 activity protects pancreatic beta cells from glucotoxicity," *Journal of Biological Chemistry*, vol. 281, no. 39, pp. 28858–28864, 2006.

[50] K. Kitani, S. Oguma, T. Nishiki et al., "A Cdk5 inhibitor enhances the induction of insulin secretion by exendin-4 both in vitro and in vivo," *Journal of Physiological Sciences*, vol. 57, no. 4, pp. 235–239, 2007.

[51] A. H. Talukder, Q. Meng, and R. Kumar, "CRIPak, a novel endogenous Pak1 inhibitor," *Oncogene*, vol. 25, no. 9, pp. 1311–1319, 2006.

[52] Z. Wang, E. Oh, and D. C. Thurmond, "Glucose-stimulated Cdc42 signaling is essential for the second phase of insulin secretion," *Journal of Biological Chemistry*, vol. 282, no. 13, pp. 9536–9546, 2007.

[53] M. Wiedemann and B. Trueb, "Characterization of a novel protein (FGFRL1) from human cartilage related to FGF receptors," *Genomics*, vol. 69, no. 2, pp. 275–279, 2000.

[54] A. A. Hardikar, B. Marcus-Samuels, E. Geras-Raaka, B. M. Raaka, and M. C. Gershengorn, "Human pancreatic precursor cells secrete FGF2 to stimulate clustering into hormone-expressing islet-like cell aggregates," *Proceedings of the National Academy of Sciences of the United States of America*, vol. 100, no. 12, pp. 7117–7122, 2003.

[55] S. Arnaud-Dabernat, M. Kritzik, A. G. Kayali et al., "FGFR3 is a negative regulator of the expansion of pancreatic epithelial cells," *Diabetes*, vol. 56, no. 1, pp. 96–106, 2007.

[56] S. D. Gerber, F. Steinberg, M. Beyeler, P. M. Villiger, and B. Trueb, "The murine Fgfrl1 receptor is essential for the development of the metanephric kidney," *Developmental Biology*, vol. 335, no. 1, pp. 106–119, 2009.

[57] C. M. Sadek, S. Jalaguier, E. P. Feeney et al., "Isolation and characterization of AINT: a novel ARNT interacting protein expressed during murine embryonic development," *Mechanisms of Development*, vol. 97, no. 1-2, pp. 13–26, 2000.

[58] C. M. Sadek, M. Pelto-Huikko, M. Tujague, K. R. Steffensen, M. Wennerholm, and J. A. Gustafsson, "TACC3 expression is tightly regulated during early differentiation," *Gene Expression Patterns*, vol. 3, no. 2, pp. 203–211, 2003.

[59] J. Qiu, Y. H. Ni, R. H. Chen et al., "Gene expression profiles of adipose tissue of obese rats after central administration of neuropeptide Y-Y5 receptor antisense oligodeoxynucleotides by cDNA microarrays," *Peptides*, vol. 29, no. 11, pp. 2052–2060, 2008.

[60] C. Vernochet, S. B. Peres, K. E. Davis et al., "C/EBPalpha and the corepressors CtBP1 and CtBP2 regulate repression of select visceral white adipose genes during induction of the brown phenotype in white adipocytes by peroxisome proliferator-activated receptor gamma agonists," *Molecular and Cellular Biology*, vol. 29, no. 17, pp. 4714–4728, 2009.

[61] R. Simon, T. Lufkin, and A. D. Bergemann, "Homeobox gene Sax2 deficiency causes an imbalance in energy homeostasis," *Developmental Dynamics*, vol. 236, no. 10, pp. 2792–2799, 2007.

[62] T. Kato, M. Emi, H. Sato et al., "Segmental copy-number gain within the region of isopentenyl diphosphate isomerase genes in sporadic amyotrophic lateral sclerosis," *Biochemical and Biophysical Research Communications*, vol. 402, no. 2, pp. 438–442, 2010.

THE JOURNAL OF BIOLOGICAL CHEMISTRY VOL. 286, NO. 23, pp. 20812–20822, June 10, 2011

Peptidyl-prolyl Cis/Trans Isomerase NIMA-interacting 1 Associates with Insulin Receptor Substrate-1 and Enhances Insulin Actions and Adipogenesis[S]

Received for publication, November 29, 2010, and in revised form, February 16, 2011 Published, JBC Papers in Press, March 17, 2011, DOI 10.1074/jbc.M110.206904

Yusuke Nakatsu[‡1], Hideyuki Sakoda[§1], Akifumi Kushiyama[¶1], Jun Zhang[‡], Hiraku Ono[§], Midori Fujishiro[§], Takako Kikuchi[§], Toshiaki Fukushima[‡], Masayasu Yoneda[‡], Haruya Ohno[‡], Nanao Horike[‖], Machi Kanna[‡], Yoshihiro Tsuchiya[‡], Hideaki Kamata[‡], Fusanori Nishimura[**], Toshiaki Isobe[‡‡], Takehide Ogihara[§§], Hideki Katagiri[§§], Yoshitomo Oka[§§], Shin-ichiro Takahashi[¶¶], Hiroki Kurihara[‖], Takafumi Uchida[‖‖], and Tomoichiro Asano[‡2]

From the [‡]Department of Medical Science, Graduate School of Medicine, University of Hiroshima, 1-2-3 Kasumi, Minami-ku, Hiroshima City, Hiroshima 734-8553, Japan, the [§]Department of Internal Medicine, Graduate School of Medicine, University of Tokyo, 7-3-1 Hongo, Bunkyo-ku, Tokyo 113-0033, the [¶]Institute for Adult Disease, Asahi Life Foundation, Tokyo 100-0006, the [**]Department of Dental Science for Health Promotion, Hiroshima University Graduate School of Biomedical Sciences, Hiroshima 734-8553, the [‡‡]Center for Priority Areas, Tokyo Metropolitan University, Hachioji, Tokyo 192-0397, Japan, the [§§]Division of Molecular Metabolism and Diabetes, Tohoku University Graduate School of Medicine, 2-1 Seiryo-machi, Aoba-ku, Sendai 980-8575, Japan, the [‖]Department of Physiological Chemistry and Metabolism, Graduate School of Medicine, University of Tokyo, 7-3-1 Hongo, Bunkyo-ku 113-0033, Tokyo, the [¶¶]Department of Applied Biological Chemistry, Graduate School of Agricultural and Life Sciences, The University of Tokyo, Bunkyo-ku, Tokyo, Japan, and the [‖‖]Department of Molecular Cell Biology, Graduate School of Agricultural Science, Tohoku University, Sendai, 113-0033 Miyagi, Japan

Peptidyl-prolyl cis/trans isomerase NIMA-interacting 1 (Pin1) is a unique enzyme that associates with the pSer/Thr-Pro motif and catalyzes cis-trans isomerization. We identified Pin1 in the immunoprecipitates of overexpressed IRS-1 with myc and FLAG tags in mouse livers and confirmed the association between IRS-1 and Pin1 by not only overexpression experiments but also endogenously in the mouse liver. The analysis using deletion- and point-mutated Pin1 and IRS-1 constructs revealed the WW domain located in the N terminus of Pin1 and Ser-434 in the SAIN (Shc and IRS-1 NPXY binding) domain of IRS-1 to be involved in their association. Subsequently, we investigated the role of Pin1 in IRS-1 mediation of insulin signaling. The overexpression of Pin1 in HepG2 cells markedly enhanced insulin-induced IRS-1 phosphorylation and its downstream events: phosphatidylinositol 3-kinase binding with IRS-1 and Akt phosphorylation. In contrast, the treatment of HepG2 cells with Pin1 siRNA or the Pin1 inhibitor Juglone suppressed these events. In good agreement with these *in vitro* data, Pin1 knock-out mice exhibited impaired insulin signaling with glucose intolerance, whereas adenoviral gene transfer of Pin1 into the *ob*/*ob* mouse liver mostly normalized insulin signaling and restored glucose tolerance. In addition, it was also demonstrated that Pin1 plays a critical role in adipose differentiation, making Pin1 knock-out mice resistant to diet-induced obesity. Importantly, Pin1 expression was shown to be up-regulated in accordance with nutrient conditions such as food intake or a high-fat diet. Taken together, these observations indicate that Pin1 binds to IRS-1 and thereby markedly enhances insulin action, essential for adipogenesis.

Peptidyl-prolyl cis/trans isomerases constitute a special class of enzymes that function not by modifying other peptides covalently but only by producing conformational changes (1–4). Pin1, one of the peptidyl-prolyl cis/trans isomerase isoforms that is distinct from the two major classes of isomerases, the cyclophilins and the FK506-binding proteins (5, 6), was initially cloned as a NIMA kinase interacting protein (7) and specifically recognizes a proline bond preceded by a phosphorylated serine or threonine residue (phospho-Ser/Thr-Pro motif) with a WW domain at its N terminus (8, 9). Then, its C-terminal PPIase domain was shown to catalyze cis-trans isomerization of the target peptidyl-prolyl bonds and thereby modify the actions of target proteins (8, 9). Since its discovery, numerous proteins have been identified as Pin1 substrates (8, 10), implicating it in the regulation of many biological processes. For example, Pin1 inhibits the phosphorylation of Cdc25 and controls the replication checkpoint in the cell cycle (11, 12). Pin1 also stabilizes the tumor suppressor p53 and is abundantly expressed in some malignant tumors, suggesting involvement in malignant transformation (13, 14). On the other hand, Pin1 is also expressed at high levels in most neurons (15, 16). Although much remains to be clarified regarding the role of Pin1 in neurons, it reportedly protects against neurodegeneration via several independent mechanisms (15, 16), as supported by the fact that Pin1 knock-out (KO) mice exhibit abnormal central nervous function (15, 16). In addition, the enzymatic function of Pin1 is reportedly inactivated by oxidative stress modification occurring in the early stages of Alzheimer disease, implicating Pin1 in brain function (16, 17). Therefore, Pin1 has been implicated in the pathogenesis of two major disorders; cancer and Alzheimer disease (9, 10).

Very recently, we reported that Pin1 expression is higher in the fed than in the fasted state and that Pin1 associates with CRTC2, a co-activator of CREB (cAMP-response element-binding protein), and suppresses CRE (cAMP-response ele-

[S] The on-line version of this article (available at http://www.jbc.org) contains supplemental Figs. 1–7.

[1] These authors contributed equally to this work.

[2] To whom correspondence should be addressed. Tel.: 81-82-257-5135; Fax: 81-82-257-5136; E-mail: asano-tky@umin.ac.jp.

ment) transcriptional activity (18). Suppressed CRE activity leads to reduced PEPCK expression and gluconeogenesis. In this study we newly identified Pin1 to be a positive regulator of insulin signaling via enhanced insulin-induced insulin receptor substrate-1 (IRS-1)[3] phosphorylation. In addition, Pin1 expression was revealed to be markedly increased by high-fat diet feeding. Because a high-fat diet is one of the most common causes of obesity, we also performed experiments to ascertain the effects of Pin1 on adipogenesis in this study. Herein, we present evidence that Pin1 plays a critical role in energy incorporation into the body by enhancing insulin signaling and adipogenesis. Our findings raise the possibility of Pin1 being a promising target molecule for treating diabetes mellitus.

EXPERIMENTAL PROCEDURES

Materials—Affinity-purified antibodies against IRS-1, IRS-2, phosphorylated tyrosine (4G10), and Akt/protein kinase B were prepared as previously described (19). Anti-Pin1 antibody was generated by immunizing rabbits with the peptide QMQKPFEDASFATRTGEMSGPVFTDSGIHIITRTE (amino acids 129–163 of human Pin1). Anti-FLAG tag antibody was purchased from Sigma, and antibodies against the p85 subunit of phosphatidylinositol 3-kinase, phospho-Ser-473 and phospho-Thr-308 of Akt, and anti-actin were from Cell Signaling Technology (Danvers, MA).

Cell Culture—Sf9 cells were grown in TC100 (Invitrogen) medium containing 10% fetal bovine serum (FBS) at 27 °C. HepG2 hepatoma cells and human preadipocyte were grown in Dulbecco's modified Eagle's medium (DMEM) containing 10% FBS at 37 °C in 5% (v/v) CO_2 in air. Mouse 3T3-L1 fibroblasts were maintained in DMEM containing 10% donor calf serum in an atmosphere of 10% CO_2 at 37 °C. Two days after the fibroblasts had reached confluence, differentiation was induced by treating the cells with DMEM containing 4 μg/ml dexamethasone, 200 nM insulin, 0.5 mmol/liter 3-isobutyl-1-methylxanthine, and 10% FBS for 48 h as described previously. Cells were fed DMEM supplemented with 10% FBS every other day and used as mature 3T3-L1 adipocytes at day 8 after the induction of differentiation.

Animals—Pin1 KO mice were generated as previously described (20), and $Pin1^{+/+}$ and $Pin1^{-/-}$ mice were obtained by breeding $Pin1^{+/-}$ mice. The genotype was determined by PCR and $Pin1^{+/-}$ mice were separated for breeding. Twelve-week-old $Pin1^{+/+}$ and $Pin1^{-/-}$ mice were fed a standard diet or high-fat diet (HFD) for 4 weeks. The nutrient composition of the standard diet was 54.4% carbohydrate, 23.6% protein, 5.3% fat with a vitamin and mineral mixture, whereas that of the HFD was 7.5% carbohydrate, 24.5% protein, 60% fat with a vitamin and mineral mixture. In other experiments, 12–16-week-old $Pin1^{+/+}$ and $Pin1^{-/-}$ mice were used.

Preparation of Adenoviruses Expressing MEF-tagged IRS Protein, Pin1, and GFP—The myc-TEV (tobacco etch virus)-FLAG (MEF) tag cassette was generated by DNA synthesis and inserted into cloning sites in the mammalian expression vector pcDNA3 (Invitrogen) and termed pcDNA3-MEF, as reported previously (19). To create the N-terminal MEF-tagged IRS-1 construct, human IRS-1 cDNA was inserted into pcDNA3-MEF. Then the coding portion of MEF-tagged IRS-1 was isolated from pcDNA3-MEF-IRS-1. Similarly, the coding regions of MEF-tagged IRS-2 and S434A IRS-1 were prepared. Recombinant adenovirus expressing MEF-tagged IRS-1, MEF-tagged S434A IRS-1, MEF-tagged IRS-2, human Pin1 with a C-terminal HA tag, GFP-tagged Pin1, and GFP were generated, and the adenovirus encoding *LacZ* served as a control. The recombinant adenoviruses expressing human Pin1 with a C-terminal HA tag and *LacZ* were used for adenoviral gene transfer into *ob/ob* mice.

Purification of MEF-tagged IRS-1-containing Complexes from Mouse Livers—Recombinant adenovirus expressing MEF-tagged IRS-1 was purified and concentrated using cesium chloride ultracentrifugation. Adenovirus encoding *LacZ* served as a control. Male C57B6 mice, 9 weeks of age, obtained from Nippon Bio-Supply Center (Tokyo, Japan), were injected via the tail vein with adenovirus at a dose of 2.5×10^7 plaque-forming units/g of body wt. Four days later, mouse livers were removed and lysed in lysis buffer (50 mM Tris-HCl, pH 7.5, 150 mM NaCl, 10% (w/v) glycerol, 100 mM NaF, 10 mM EGTA, 1 mM Na_3VO_4, 1% (w/v) Triton X-100, 5 μM $ZnCl_2$, 2 mM PMSF, 10 μg/ml aprotinin, and 1 μg/ml leupeptin). Lysates were centrifuged at 100,000 × *g* for 20 min at 4 °C. Supernatants were passed through a 5-μm filter, incubated with 150 μl of Sepharose beads for 60 min at 4 °C, and then passed through a 0.65-μm filter. The filtrated supernatant was mixed with 150 μl of anti-myc-conjugated Sepharose beads for the first immunoprecipitation. After incubation for 90 min at 4 °C, the beads were washed 5 times with 1.5 ml of TNTG buffer (20 mM Tris-HCl, pH 7.5, 150 mM NaCl, 10% (w/v) glycerol, and 0.1% (w/v) Triton X-100), twice with buffer A (20 mM Tris-HCl, pH 7.5, 150 mM NaCl, and 0.1% (w/v) Triton X-100), and finally once with TNT buffer (50 mM Tris-HCl, pH 8.0, 150 mM NaCl, and 0.1% (w/v) Triton X-100). The washed beads were incubated with 15 units of tobacco etch virus protease (Invitrogen) in 150 μl of TNT buffer to release bound materials from the beads. After incubation for 60 min at room temperature, supernatants were pooled, and the beads were washed twice with 75 μl of buffer A. The resulting supernatants were combined and incubated with 25 μl of FLAG-Sepharose beads for the second immunoprecipitation. After a 60-min incubation at room temperature, the beads were washed 3 times with 500 μl of buffer A, and proteins bound to the FLAG beads were dissociated by incubation with 1 mM synthetic FLAG peptides in buffer A for 120 min at 4 °C. Approximately 3 μg of protein (0.01% of starting materials) were routinely recovered by this procedure. The samples were electrophoresed and subjected to SDS-PAGE and immunoblotting.

Immunoprecipitation and Immunoblotting—The cells were solubilized with Laemmli buffer (0.2 M Tris-HCl, 4% SDS, 10% glycerol, 5% 2-mercaptoethanol, 0.1% bromphenol blue). Equal amounts of protein from whole cell lysates were resolved by SDS-PAGE. Then the proteins were transferred to polyvinylidene difluoride membranes (Millipore, Billerica, MA) using an electroblotting apparatus (Mighty Small

[3] The abbreviations used are: IRS-1, insulin receptor substrate-1; HFD, high-fat diet; SAIN, Shc and IRS-1 NPXY binding; PPAR, peroxisome proliferator-activated receptor; MEF, myc-TEV (tobacco etch virus)-Flag.